ADVANCED MATERIALS
www.advmat.de

Check for updates

Scleral Lens Sensor for Ocular Electrolyte Analysis

Ali K. Yetisen, Nan Jiang, Carmen M. Castaneda Gonzalez, Zeynep Izlen Erenoglu, Jie Dong, Xingchen Dong, Simon Stößer, Martin Brischwein, Haider Butt, Maria F. Cordeiro, Martin Jakobi, Oliver Hayden, and Alexander W. Koch*

The quantitative analysis of tear analytes in point-of-care settings can enable early diagnosis of ocular diseases. Here, a fluorescent scleral lens sensor is developed to quantitatively measure physiological levels of pH, Na^+, K^+, Ca^{2+}, Mg^{2+}, and Zn^{2+} ions. Benzenedicarboxylic acid, a pH probe, displays a sensitivity of 0.12 pH units within pH 7.0–8.0. Crown ether derivatives exhibit selectivity to Na^+ and K^+ ions within detection ranges of 0–100 and 0–50 mmol L^{-1}, and selectivities of 15.6 and 8.1 mmol L^{-1}, respectively. A 1,2 bis(*o*-aminophenoxy)ethane-*N*,*N*,-*N*′,*N*′-tetraacetic-acid-based probe allows Ca^{2+} ion sensing with 0.02–0.05 mmol L^{-1} sensitivity within 0.50–1.25 mmol L^{-1} detection range. 5-Oxazolecarboxylic acid senses Mg^{2+} ions, exhibiting a sensitivity of 0.10–0.44 mmol L^{-1} within the range of 0.5–0.8 mmol L^{-1}. The *N*-(2-methoxyphenyl)iminodiacetate Zn^{2+} ion sensor has a sensitivity of 1 µmol L^{-1} within the range of 10–20 µmol L^{-1}. The fluorescent sensors are subsequently multiplexed in the concavities of an engraved scleral lens. A handheld ophthalmic readout device comprising light-emitting diodes (LEDs) and bandpass filters is fabricated to excite as well as read the scleral sensor. A smartphone camera application and an user interface are developed to deliver quantitative measurements with data deconvolution. The ophthalmic system enables the assessment of dry eye severity stages and the differentiation of its subtypes.

Deficiency in tear production or tear evaporation causes dry eye syndrome and results in hyperosmolarity which leads to symptoms of discomfort and corneal abrasion.[1] While most of the dry eye treatment has focused on deficiency in tear production and inflammation, recently, meibomian gland dysfunction (MGD) has been identified as the major cause of dry eye disease.[2] Another common cause of dry eye disease is inadequate tear production from lacrimal hyposecretion, often decreasing with age, resulting in aqueous tear deficiency.[3] Other causes include congenital alacrima,[4] xerophthalmia,[5] lacrimal gland ablation,[6] sensory denervation,[7] laser-assisted in situ keratomileusis (LASIK),[8] and refractive surgeries.[9] Rare cases may be due to Sjögren's syndrome,[10] polychondritis,[11] rheumatoid arthritis,[12] Wegener's granulomatosis,[13] and systemic lupus erythematosus,[14] and autoimmune diseases.[15] Postmenopausal women[16] and diabetics[17] are at increased risk of dry eye disease.

Existing dry eye diagnostic approach is primarily based on identifying symptoms such as feeling dry, gritty or sandy sensation, burning, and red eyes.[13] Examination of the ocular surface with a slit lamp and symptom questionnaires are the most common diagnosis approaches.[18] Other approaches include Schirmer's test for measuring the tear fluid volume,[19] fluorescein staining to determine epithelial damage,[20] and break-up test to

Dr. A. K. Yetisen, C. M. Castaneda Gonzalez, Z. I. Erenoglu, J. Dong, X. Dong, S. Stößer, Dr. M. Jakobi, Prof. A. W. Koch
Institute for Measurement Systems and Sensor Technology
Technical University of Munich
Munich D-80290, Germany
E-mail: a.k.yetisen@tum.de

Dr. N. Jiang
School of Engineering and Applied Sciences
Harvard University
Cambridge, MA 02138, USA

Dr. M. Brischwein, Prof. O. Hayden
Department of Electrical and Computer Engineering
TranslaTUM Campus
Technical University of Munich
Munich D-80290, Germany

The ORCID identification number(s) for the author(s) of this article can be found under https://doi.org/10.1002/adma.201906762.

© 2019 The Authors. Published by WILEY-VCH Verlag GmbH & Co. KGaA, Weinheim. This is an open access article under the terms of the Creative Commons Attribution License, which permits use, distribution and reproduction in any medium, provided the original work is properly cited.

DOI: 10.1002/adma.201906762

Prof. H. Butt
Department of Mechanical Engineering
Khalifa University
127788 Abu Dhabi, United Arab Emirates

Prof. M. F. Cordeiro
The Western Eye Hospital
Imperial College Healthcare NHS Trust
London NW1 5QH, UK

Prof. M. F. Cordeiro
The Imperial College Ophthalmic Research Group (ICORG)
Imperial College
London NW1 5QH, UK

Prof. M. F. Cordeiro
Glaucoma and Retinal Neurodegeneration Group
Department of Visual Neuroscience
UCL Institute of Ophthalmology
London EC1V 9EL, UK

measure tear evaporation.[21] However, they lack the specificity to identify the underlying causes of dry eye. Measurements of tear hyperosmolarity,[22] e.g., osmometers (TearLab), have large degree of variations, and readings are difficult to interpret.[23] Furthermore, lateral-flow assays such as InflammaDry (Rapid Pathogen Screening),[24] Tearscan (Advanced Tear Diagnostics)[25] can test matrix metalloproteinase-9 and lactoferrin. These analytes are not specific for dry eye syndrome, and can be due to different etiological causes of dry eye syndrome. Additionally, LipiView (TearScience), a benchtop digital interferometry imaging device, is used for monitoring the lipid layer of a patient's eye.[26] However, this high-cost technology produces erroneous results when a patient's blinking rate is inconsistent.

Progressive deterioration of ocular surface, resulting in scarring and impaired vision can be prevented by early detection of dry eye.[27] When dry eye is diagnosed at an early stage, aggressive treatments can be implemented to protect the cornea,[28] expel blockages in meibomian glands,[29] and reduce inflammation.[30] The differentiation between MGD and lacrimal gland dysfunction (LGD) and their severity stages can allow the optimization of dry eye treatment and management.[31] For example, while LGD can be treated with lubricating eye drops, MGD requires unclogging the glands by heat treatment.[32] Quantitative determination of electrolyte composition in tear fluid can enable new personalized treatments and allow the evaluation of treatment efficacy. Additionally, diagnosing early-stage dry eye has clinical utility prior or post refractive/LASIK eye surgeries since it can affect the surgical outcomes and progresses to the mild dry eye.[33] Additionally, dry eye syndrome is a leading reason for discontinuing contact lens use,[34] and early diagnosis can help the ophthalmologist to choose the right lens type and formulation. Therefore, the accurate differentiation of dry eye subtypes can provide a diagnostic utility. A potential approach to dry eye severity assessment and subtype differentiation is through the measurements of tear electrolytes, in which the composition differs based on the dry eye subtype. Sensing tear electrolytes can provide quantitative data to diagnose and track the course of dry eye syndrome, manage the eye drop medication dosage, as well as create a diagnostic basis for personalized eye drops.[35]

Contact lenses are widely used for vision correction (refractive errors), therapeutic, and cosmetic purposes.[36] The first poly(methyl methacrylate) (PMMA) hard contact lenses were developed.[37] The limitations in the biocompatibility of these rigid contact lenses was eliminated with hydrogel contact lenses made of poly(2-hydroxyethyl methacrylate (pHEMA) in the 1970s. These polymeric materials have formed the basis of sensing technologies embedded into electronic contact lenses. Current electronic contact lens sensors focused on monitoring ocular dimensional changes for intraocular pressure (IOP) measurements for glaucoma diagnosis or sensing glucose in tear fluid for the management of diabetes. To continually record the IOP, an electronic soft contact lens was developed to measure and send ocular dimensional changes wirelessly to a data recording device through an antenna.[38] However, this product had limited clinical utility due to the poor relationship between pressure (mmHg) and an electrically measured value. To measure the glucose concentration on a contact lens, the glucose oxidase reaction was employed in an electrochemical assay.[39] However, the concentration of glucose in tear fluid is not correlated with blood glucose, limiting the potential clinical utility of these electrochemical contact lenses. In contrast with the electronic contact lenses, optical sensors do not require electrical components such as data transmission units and power supply; hence, their integration in contact lenses can offer an advantageous diagnostic platform in point-of-care settings.

Dry eye patients generally do not tolerate wearing soft contact lenses. Thus, fluorosilicone acrylate scleral lenses are prescribed to patients with severe dry eye syndrome.[40] Scleral lenses are widely used in the ophthalmology clinics to treat ocular surface disease such as dry eye syndrome. When integrated with sensors, the scleral lenses sensors can be used in point-of-care settings to: i) monitor tear electrolytes to diagnose the severity and subtypes of dry eye syndrome, ii) quantitatively assess the treatment efficacy, and iii) personalize the formulation of eye drops based on a patient's eye condition. Such scleral lens sensors can allow continual monitoring of the ocular physiology toward continuous tear biomarker analyses in personalized medicine.

Here, a minimally invasive multiplexed scleral lens sensor was developed to measure electrolyte concentrations in tear film for dry eye diagnosis in point-of-care settings. The scleral lens sensor consisted of fluorescent probes to quantitatively measure pH value and electrolyte (Na^+, K^+, Ca^{2+}, Mg^{2+}, and Zn^{2+} ions) concentrations within the physiological range. To multiplex the fluorescent probes, a scleral lens was engraved using a CO_2 laser to produce concavities.[41] A leak-proof scleral lens was fabricated by bonding a silicone hydrogel membrane to create fully enclosed microfluidic channels and concavities. The enclosed scleral lens assembly prevented the evaporation of aqueous fluorescent probes and artificial tear fluid while allowing the diffusion of electrolytes into the multiplexed sensing regions. A readout platform comprising an imaging unit with LEDs and optical filters was developed to obtain quantitative measurements with the aid of a smartphone camera. A smartphone algorithm and a user interface were coded to obtain quantitative diagnostic data from the scleral lens sensor. A data deconvolution algorithm was developed to compensate for the measurement errors by analyzing multiple sensor readouts. Artificial tear fluids that mimic tear composition in dry eye syndrome were utilized to obtain quantitative electrolyte measurements. The integrated scleral lens sensor and the smartphone readout system allow for the diagnosis of dry eye severity stages and subtypes in point-of-care settings. The present work demonstrates an integrated ophthalmic system to quantitatively analyze and report dry eye disease for in vivo diagnostics.

The pH value of tear fluid increases up to 7.9 in patients with dry eye syndrome as compared to pH 7.4 in healthy individuals (Tables S1 and S2, Supporting Information).[35] Thus, determining the pH value of tear fluid has clinical utility in the diagnosis of dry eye syndrome. A pH sensor should be able to detect changes in at least 0.5 pH units to provide clinically useful data. Benzenedicarboxylic acid (BDCA) was used as fluorescent pH probe (pK_a 7.5) for optical measurements. The emission wavelengths of BDCA experience a pH-dependent shift from yellow-orange ($\lambda = 580$ nm) to deep red ($\lambda = 640$ nm) fluorescence due to deprotonation of its phenolic substituent (**Figure 1**a, Figure S1a, Supporting Information). As the concentration of BDCA increased from 5 to 100 μmol L^{-1} at a constant pH value (7.4), the relative fluorescence intensity increased sixfold (Figure 1b). The fluorescence

© 2019 The Authors. Published by WILEY-VCH Verlag GmbH & Co. KGaA, Weinheim

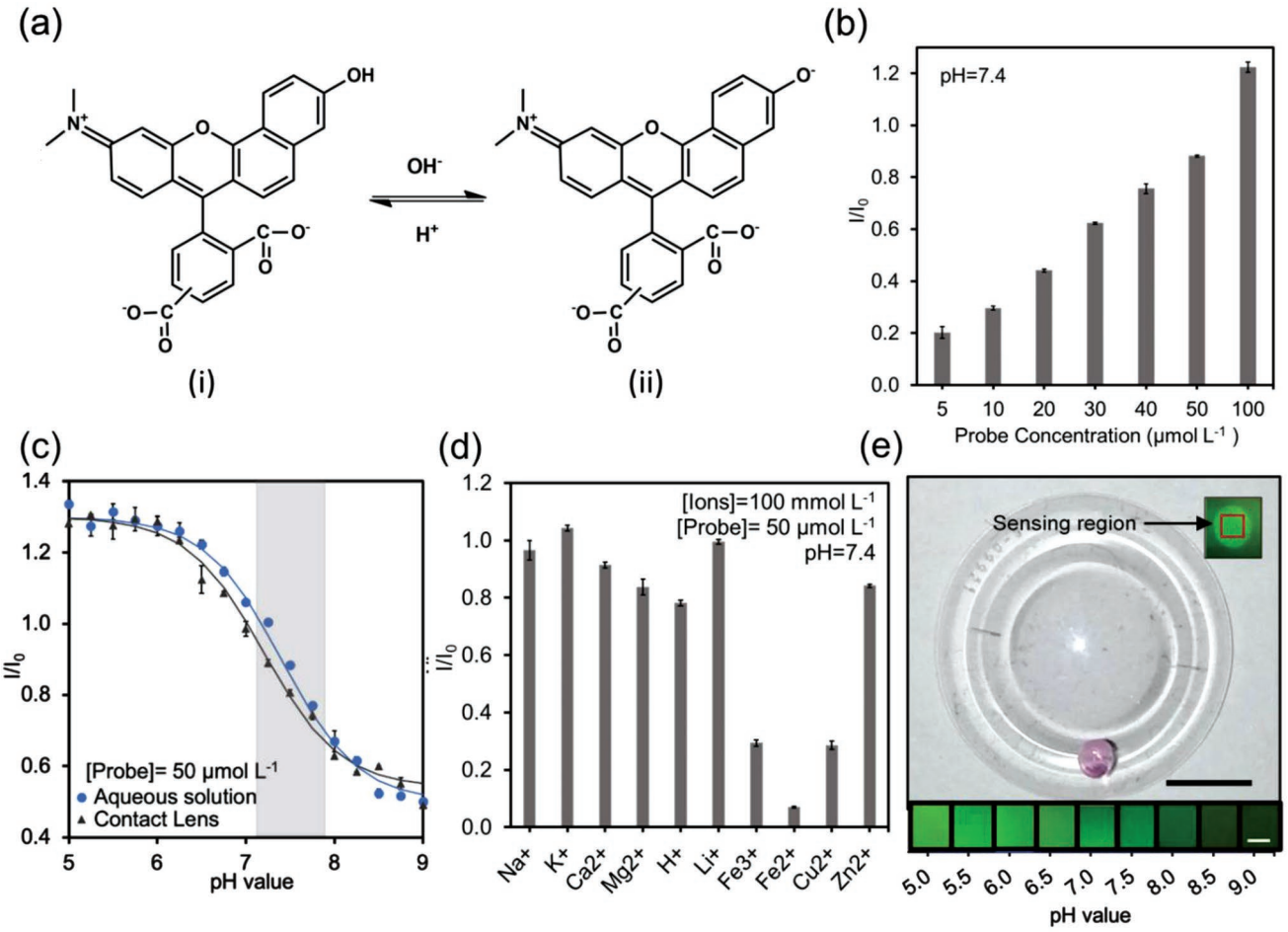


Figure 1. Quantification of pH values in tris buffer solutions (150 mmol L^{-1}) at 24 °C. a) Principle of operation of fluorescent BDCA: i) phenolic form (HA) and ii) phenolate form (A^-). b) Fluorescence intensity readouts as the concentration of BDCA ($\lambda_{ex}/\lambda_{em}$:520/590 nm) was varied from 5–100 μmol L^{-1} at pH = 7.4 in aqueous solutions ($n = 3$). c) Quantification of tris buffer pH (150 mmol L^{-1}) in a 96-well plate and on a scleral lens at a constant BDCA concentration (50 μmol L^{-1}). Curves were fitted using Equation (1). ($n = 3$). Shadows represent the physiological range of the pH value in tear fluid. d) Relative fluorescence intensity readouts of mono/divalent ions at a constant BDCA concentration (50 μmol L^{-1}) at pH 7.4 ($n = 3$). e) Photograph of a scleral lens with one concavity functionalized with BDCA (50 μmol L^{-1}, 2 μL). The color scale represents fluorescence images of tris buffer solutions (pH 5–9) mixed (1:1, v/v) with BDCA (50 μmol L^{-1}), excited with an LED (505 nm) and filtered with a bandpass optical filter (580 nm, FWHM = 10 ± 2 nm). The red square in the inset shows the fluorescent sensing region of the scleral lens sensor. Scale bar = 5 mm, inset scale bar = 1 mm. Error bars represent standard deviation of the mean.

intensity decreased 2.7-fold as the pH value of tris buffer increased from 5.0 to 9.0, where the BDCA concentration was constant (50 μmol L^{-1}) (Figure 1c). This behavior can be explained by the Henderson–Hasselbalch equation[42]

$$\log_{10}\left(\frac{\alpha}{1-\alpha}\right) = \mathrm{pH} - \mathrm{p}K_a \quad (1)$$

where α is the degree of dissociation for acids.[43] The sigmoid dose-response curve was used to assess the equation of the I/I_0-pH curve between pH 5.0 and 9.0, showing a pK_a value of ≈7.4. I refers to the measured fluorescence emission, and I_0 represents the fluorescence emission of the control sample. The fluorescence intensity decrease (1.6-fold) between pH 7.0 and 8.0 corresponds to a sensitivity of 0.12 pH units.

The effect of different electrolytes (100 mmol L^{-1}) on BDCA probe response (50 μmol L^{-1}, pH 7.4) was tested (Figure 1d). In the presence of Na^+, K^+, Ca^{2+}, Mg^{2+}, Li^+, and Zn^{2+} ions (100 mmol L^{-1}), the fluorescence intensity of the BDCA increased by 18%, 31%, 12%, 2%, 25%, and 1%, respectively. However, in the presence of Fe^{3+} Fe^{2+}, and Cu^{2+} ions (100 mmol L^{-1}), the fluorescence intensity of the BDCA decreased by 56%, 87%, and 56%, respectively. Figure 1e shows a scleral lens sensor with an engraved concavity by CO_2 laser ablation. The concavity was functionalized with the pH probe (2 μL, 50 μmol L^{-1}) and tested in tris buffer solutions (pH 5.0–9.0). The pH probe was excited by an LED (505 nm) and the fluorescence emission was filtered by a bandpass filter (580 nm) (Figure 1e). The light intensity values were analyzed with an image-processing algorithm in MATLAB. The fluorescence intensity decreased as the pH value of the solution increased in the scleral lens sensor, which was consistent with the measurements conducted in aqueous solutions (Figure 1c,e).

In dry eye syndrome, Na^+ ion concentration reaches up to 136.1 mmol L^{-1} in MGD, 142.2 mmol L^{-1} in LGD, and

© 2019 The Authors. Published by WILEY-VCH Verlag GmbH & Co. KGaA, Weinheim

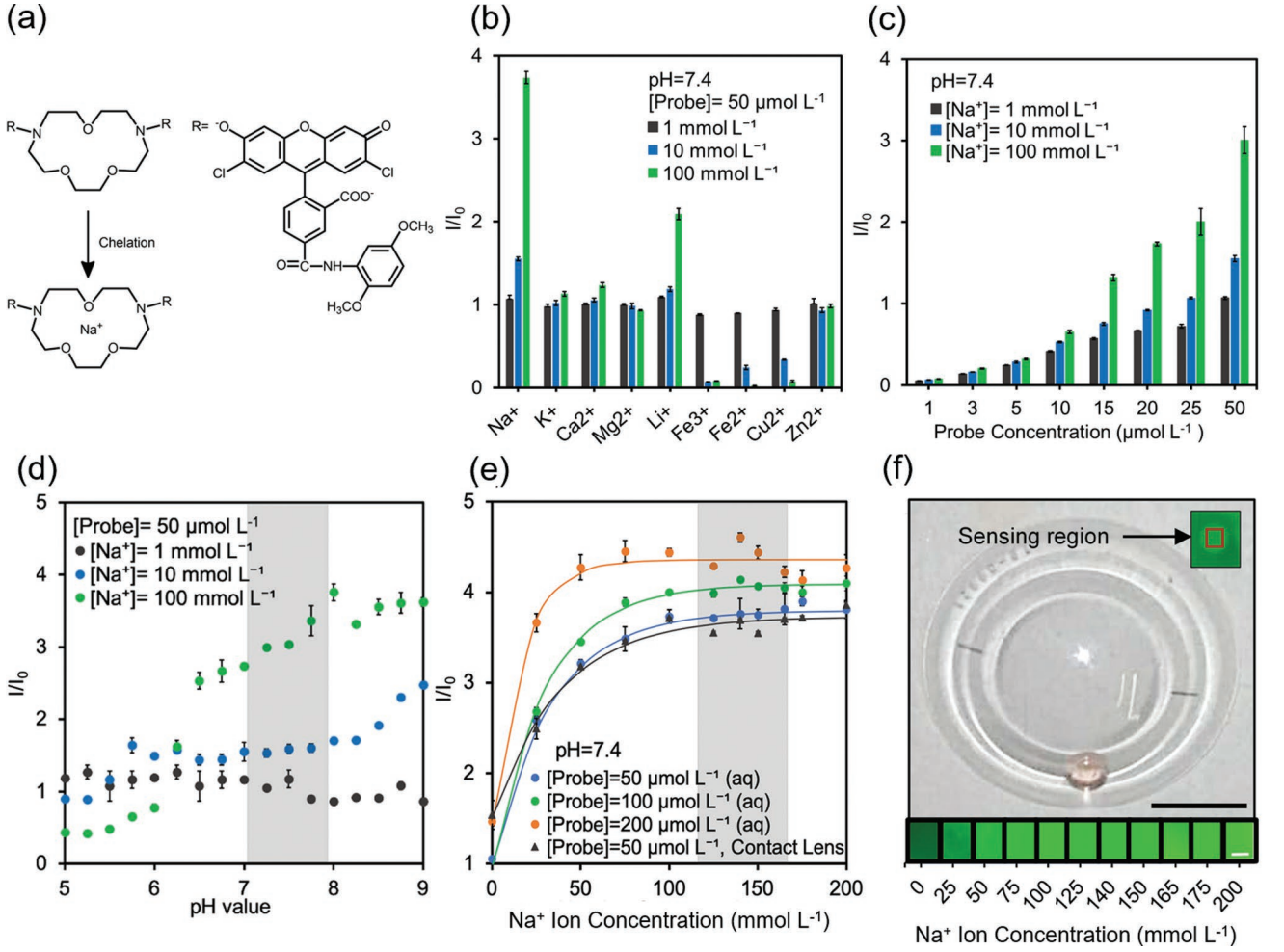


Figure 2. Quantification of Na^+ ions using DA15C5 in tris buffer solutions (150 mmol L^{-1}) at 24 °C. a) Chelation process of DA15C5 with Na^+ ions. b) Fluorescence readouts of DA15C5 ($\lambda_{ex/em}$: 492/520 nm, 50 µmol L^{-1}) in aqueous electrolyte solutions (1–100 mmol L^{-1}, pH 7.4) ($n = 3$). c) Quantification of DA15C5 concentration in the presence of Na^+ ions (1–100 mmol L^{-1}, pH 7.4) ($n = 3$). d) The effect of pH variation on DA15C5 in tris buffer solutions of pH 4.0–9.0 (150 mmol L^{-1}) with Na^+ concentrations (1–100 mmol L^{-1}) ($n = 3$). e) Fluorescence readouts of DA15C5 (50–200 µmol L^{-1}) in aqueous Na^+ ion solutions and on the scleral lens sensor with varying concentrations at pH 7.4 ($n = 3$). Curves were fitted using Equation (2). f) Photograph of DA15C5 (50 µmol L^{-1}, 2 µL) in a single concavity of the scleral lens. The color scale represents the fluorescence intensities of DA15C5 (50 µmol L^{-1}) mixed (1:1, v/v) with Na^+ ion solutions, excited with 505 nm LED and filtered by 530 nm bandpass filter (FWHM = 10 ± 2 nm). The inset shows the fluorescence images of the sensing region on the scleral lens sensor. Scale bar = 5 mm, inset scale bar = 1 mm. Shadows in (d,e) represent the physiological ranges of pH and Na^+ ion concentrations in human tears. Error bars represent standard deviation of the mean.

145.1 mmol L^{-1} in MGD/LGD type dry eye syndrome.[44] Crown ethers are cyclic chemical compounds containing negatively charged oxygen atoms that form hydrogen bonds with the metal ions.[45] By incorporating fluorescent substituents into the crown ether, the changes induced by bound ions can be quantified by measuring fluorescence emission changes. The Na^+ ion probe consists of a 2′,7′-dichlorofluorescein dye connected to each of the nitrogen atoms in the diaza-15-crown-5 (DA15C5) with a cavity size of 0.17–0.22 nm, which is selective for Na^+ ions (**Figure 2**a, Figure S1, Supporting Information). Upon binding to Na^+ ions, fluorescence emission increases.[46] The peak excitation and emission wavelengths for DA15C5 are 507 and 532 nm, respectively.[47]

The selectivity of the DA15C5 sensor (50 µmol L^{-1}) to Na^+ ions and other electrolytes was measured in tris buffer solutions (Figure 2b). Na^+ ions exhibited the highest fluorescence intensity in all the probe concentrations. The relative fluorescence intensity of DA15C5 in response to Na^+ ions (100 mmol L^{-1}, pH 7.4) was 3.5, 3.2, 4.2 folds higher than that of K^+, Ca^{2+}, and Mg^{2+} ions (100 mmol L^{-1}), respectively. The DA15C5 bonded selectively to Na^+ ions in concentrations above 10 mmol L^{-1}, which also corresponds to the physiological Na^+ ion concentration in the tear fluid (Tables S1 and S2, Supporting Information). As the concentration of Na^+ ions decreased from 100 to 1 mmol L^{-1}, the relative fluorescence intensity of the DA15C5 decreased by 58% (Figure 2b). Fe^{3+}, Fe^{2+}, and Cu^{2+} ions in concentrations of 100 and 10 mmol L^{-1} decreased the relative fluorescence intensity due to quenching effect; however, these ions at 1 mmol L^{-1} concentration had a subtle fluorescence response. Subsequently, the variation of DA15C5 probe concentration on the fluorescence readouts was tested. The concentration of DA15C5 in tris buffer was

© 2019 The Authors. Published by WILEY-VCH Verlag GmbH & Co. KGaA, Weinheim

increased from 1 to 50 µmol L^{-1} as the Na^+ ion concentration was kept constant. The fluorescence intensity increased 37, 22, and 19 folds with increasing DA15C5 concentration for all ionic strength values (1–100 mmol L^{-1}), respectively (Figure 2c). Additionally, the effect of the pH value on the Na^+ ion probe response was assessed (Figure 2d). DA15C5 (50 µmol L^{-1}) was mixed with Na^+ ions (1–100 mmol L^{-1}) in tris buffer (pH 5.0–9.0, 150 mmol L^{-1}). The fluorescence intensities for 1 and 10 mmol L^{-1} of the Na^+ ion concentrations were pH invariant, whereas the increase of pH with 100 mmol L^{-1} Na^+ solution resulted in a 24% increase in fluorescence intensity. This indicated that the pH value of the solution did not cause significant interference in physiological conditions.

The emission intensity of DA15C5 (50–200 µmol L^{-1}, pH 7.4) was measured in Na^+ ion solutions (25–200 mmol L^{-1}) in tris buffer (pH 7.4) (Figure 2e). As the Na^+ ion concentration increased, the fluorescence intensity increased 2.9, 3.6, and 4.3 folds for 50, 100, and 200 µmol L^{-1} probe concentrations, respectively. The concentration-dependent fluorescence intensity can be expressed as

$$I'(C) = \frac{I(C)}{I_0(C)} = I'_s\left(1 - e^{-\alpha C}\right) \quad (2)$$

where I_s' indicates the saturated relative fluorecence intensity, α is the saturation decay constant, and C is the ion concentration of the solution. The dissociation constant K_d of DA15C5 was calculated to be 5.5 mmol L^{-1} determined by

$$\left[Na^+\right]_{free} = K_d \cdot \frac{F - F_{min}}{F_{max} - F} \quad (3)$$

where $[Na^+]_{free}$ is the known Na^+ ion concentration in solution, F is the fluorescence intensity measured at this known Na^+ ion concentration, F_{min} is the fluorescence intensity in a Na^+ ion free solution and F_{max} is the saturation fluorescence intensity at high Na^+ ion concentrations.

DA15C5 (50 µmol L^{-1}) was immobilized on a scleral lens with a concavity and mixed with Na^+ ion solutions (0–200 mmol L^{-1}). The scleral lens was excited with a 505 nm LED and the light was filtered out with a 530 nm bandpass optical filter. Figure 2f shows the photographs of the sensing regions in the scleral lens sensor exposed to Na^+ ion solutions. The intensity values were analyzed with an image-processing algorithm in MATLAB. The intensity of the probe on the scleral lens increased as the Na^+ ion concentration increased (Figure 2e), which indicated that the measurements on the scleral lens and in the microplate reader were consistent.

The Na^+ ion concentration in tear fluid increases by 2.2% from 133.2 to 136.1 mmol L^{-1} in MGD, by 6.7% from 133.2 to 142.2 mmol L^{-1} in LGD, and by 8.9% from 133.2 to 145.1 mmol L^{-1} in the presence of both MGD and LGD, which corresponds to a required Na^+ ion probe sensitivity of 3–12 mmol L^{-1} to provide clinically useful data.[44] The sensitivity of the Na^+ ion probe in the entire test range of ion concentrations was calculated to be 15.6 mmol L^{-1}. The sensitivity in the linear range of the plot until 100 mmol L^{-1} Na^+ ions was determined to be 6.7 mmol L^{-1}. DA15C5 was stable in the physiological range of the pH and responded to Na^+ ion concentrations less than 100 mmol L^{-1}.

The K^+ ion concentration in tear film ranges between 20 and 42 mmol L^{-1} with an average value of 24.0 mmol L^{-1} (Table S1, Supporting Information).[44] The K^+ ion concentration in the tear film rises up to 24.6 mmol L^{-1} in MGD, 24.9 mmol L^{-1} in LGD, and 25.4 mmol L^{-1} in the presence of MGD/LGD (Table S2, Supporting Information). DA18C6 is a fluorescent chelating crown ether, containing benzofuranyl fluorophores linked to the nitrogen atoms of the crown ether, which has a cavity size of 0.26–0.32 nm (**Figure 3**a). This specific size ensures the selectivity of the probe against K^+ ions, corresponding to the 275 pm van der Waals radii. Excited with 340/380 nm light, the fluorescence emission peak of DA18C6 and K^+ ion complex increases (λ_{em} = 500 nm) (Figure S1, Supporting Information). The fluorescence response of DA18C6 in the presence of electrolytes was investigated at different concentrations (1–100 mmol L^{-1}) (Figure 3b). K^+ ions exhibited the highest fluorescence intensity in all measurements. The relative fluorescence intensity of DA18C6 in response to K^+ ions (100 mmol L^{-1}, pH 7.4) was 2.0, 3.5, 9.8 folds higher than that of Na^+, Ca^{2+}, and Mg^{2+} ions (100 mmol L^{-1}), respectively. The relative fluorescence intensity of DA18C6 (50 µmol L^{-1}) in response to K^+ ions at 20, 10, and 1 mmol L^{-1} was 2.9, 2.8, 4.8 folds higher than that of Na^+ ions at equivalent concentrations, respectively. This is due to the small van der Waals radius of Na^+ ions at 227 pm.[48]

As the concentration of DA18C6 complexing agent increased (from 1 to 50 µmol L^{-1}), the relative fluorescence intensity of K^+ ion complex increased by 12, 15, 11, and 5 folds for 100, 20, 10, and 1 mmol L^{-1} of K^+ ion solutions, respectively (Figure 3c). Fluorescence intensities for K^+ ions (1–100 mmol L^{-1}) changed with pH variance in tris buffer (150 mmol L^{-1}, pH 4.0–9.0), but remained constant within the physiological range (pH 7.0–8.0) (Figure 3d). K^+ ion concentration variation was tested with DA18C6 (1–100 µmol L^{-1}) using K^+ solutions in tris buffer (pH 7.4, 150 mmol L^{-1}) both in aqueous solutions and on a scleral lens sensor with different ionic strength values (2.5–50 mmol L^{-1}). As the K^+ ion concentration increased, the fluorescence intensity increased 2.0, 5.7, 8.6, and 8.1-folds, for 1, 10, 50, and 100 µmol L^{-1} DA18C6 concentrations, respectively (Figure 3e). The K_d value of the K^+ sensor was calculated as 8.13 mmol L^{-1} using Equation (3) (Figure 3e), which was comparable with the reported K_d of 8 mmol L^{-1}.[48]

Figure 3f shows a photograph of a scleral lens sensor with a concavity, which was engraved by CO_2 laser ablation. DA18C6 (2 µL, 50 µmol L^{-1}) was immobilized in the concavity of the scleral lens sensor. Solutions containing K^+ ions (0–50 mmol L^{-1}) were tested on the concavity on the scleral lens. The scleral lens was excited with a UV-LED (340 nm) and photographs of the scleral lens were taken using a 500 nm bandpass filter. The light intensity values were analyzed with an image-processing algorithm in MATLAB. Figure 3e shows measurement results in scleral lens sensors, comparable to the result in aqueous solutions (50 µmol L^{-1}).

The K^+ ion concentration in the tears increases in both MGD and LGD. Therefore, a feasible biosensor should be sensitive to changes of 0.6, 0.9, and 1.4 mmol L^{-1} for the detection of MGD, LGD, and MGD/LGD, respectively. The sensitivity of DA18C6 to K^+ ions was calculated as 0.8 mmol L^{-1}. In general, DA18C6 showed high selectivity for K^+ ions, was pH invariant over the physiological range for all ionic strength values of K^+ ion solutions.

© 2019 The Authors. Published by WILEY-VCH Verlag GmbH & Co. KGaA, Weinheim

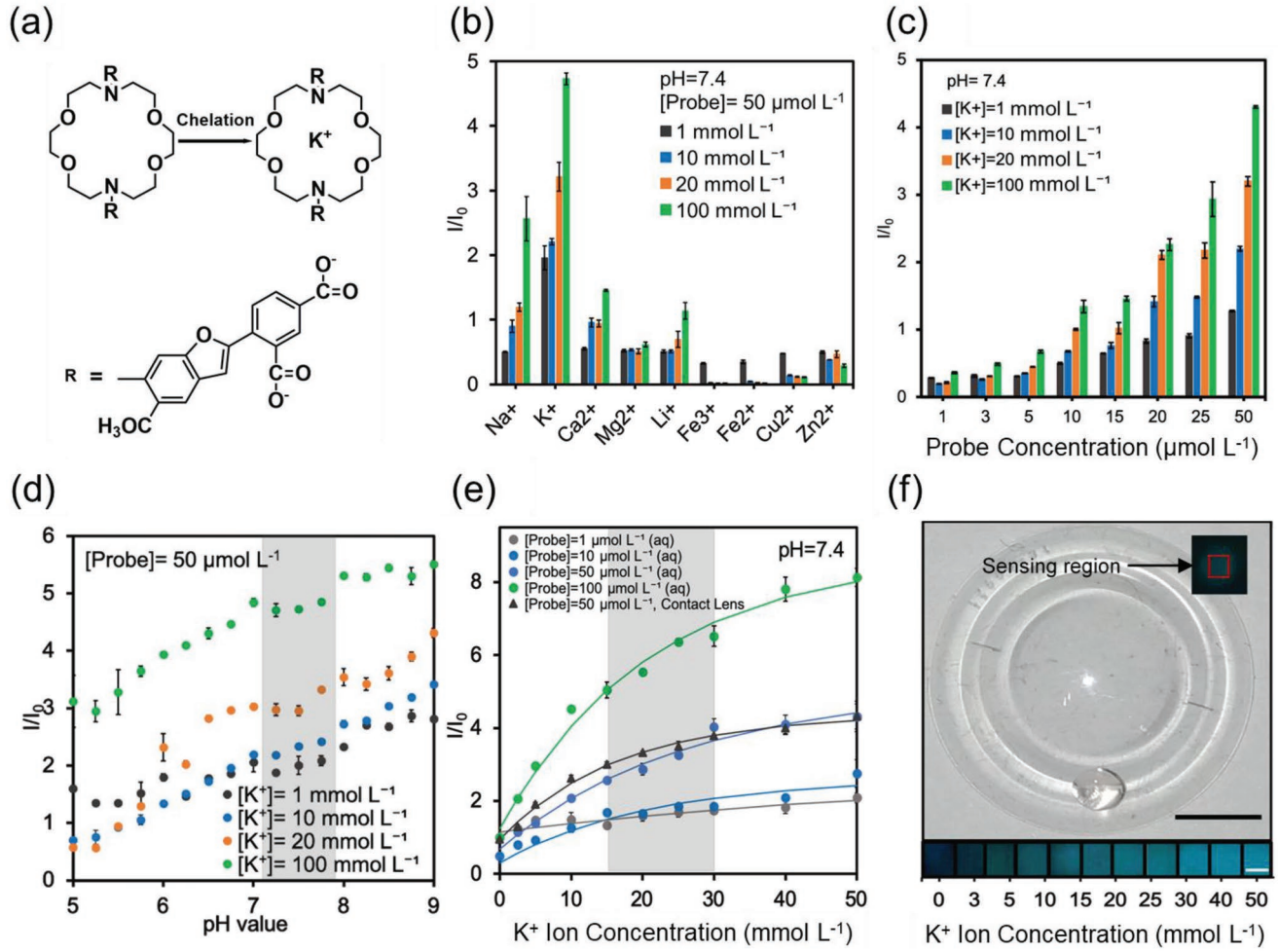


Figure 3. Quantification of K^+ ions using DA18C6 in tris buffer solutions (150 mmol L^{-1}) at 24 °C. a) Chelation mechanism of DA18C6 with a K^+ ion. b) Fluorescence intensity readouts of DA18C6 complex ($\lambda_{ex/em}$: 340/505 nm, 50 µmol L^{-1}) in aqueous electrolyte solutions (1–100 mmol L^{-1}) at pH 7.4 ($n = 3$). c) The effect of varying the DA18C6 concentration in the presence of K^+ ions (1–100 mmol L^{-1}) in buffer solutions of pH 7.4 ($n = 3$). d) The effect of pH on fluorescence intensities of DA18C6 in tris buffer solutions (150 mmol L^{-1}) between pH 4.0–9.0 with K^+ ion concentrations (1–100 mmol L^{-1}) ($n = 3$). e) Fluorescence readouts of DA18C6 (1–100 µmol L^{-1}) in aqueous solutions and on a scleral lens with varying concentrations of K^+ ions (tris buffer, 150 mmol L^{-1} pH 7.4) ($n = 3$). Curves were fitted using Equation (2). f) Photograph of an engraved scleral lens with DA18C6 (2 µl, 50 µmol L^{-1}). The inset shows the fluorescence sensing region of the scleral lens. The color scale represents the fluorescence intensity of DA18C6 complex with varying K^+ ion concentrations excited with 340 nm LED and filtered with a 500 nm bandpass filter (FWHM = 40 ± 8 nm). Scale bar = 5 mm, inset scale bar = 1 mm. Shadows in (d,e) represent the physiological range of pH and K^+ ion concentrations in the human tear film. Error bars represent standard deviation of the mean.

Ca^{2+} ion concentration in tears lies between 0.4 and 1.1 mmol L^{-1} (Table S1, Supporting Information). The healthy human eye has a Ca^{2+} ion concentration of 0.8 mmol L^{-1}, whereas dry eye syndrome results in an elevated Ca^{2+} ion concentration (Table S2, Supporting Information). By quantifying Ca^{2+} ion concentrations, the severity stage of dry eye can be assessed. In a mild stage of dry eye syndrome, the concentration of Ca^{2+} ions in tear fluid increases 6.25% (0.85 mmol L^{-1}), moderate stages show an increase of 12.5% (0.90 mmol L^{-1}), and a severe stage is characterized by an increase of 18.75% (0.95 mmol L^{-1}) (Table S3, Supporting Information). To differentiate between the severity stages of dry eye syndrome, a sensor sensitivity of 0.05 mmol L^{-1} is required. Additionally, MGD and LGD can be differentiated. An increase of 2.5% (0.82 mmol L^{-1}) is related to MGD, whereas an increase of 5% (0.84 mmol L^{-1}) is attributed to LGD. Having a Ca^{2+} ion concentration of 0.86 mmol L^{-1} (7.5% increase) is a sign of both MGD and LGD subtypes of dry eye syndrome (Table S2, Supporting Information). To characterize dry eye subtype, a probe sensitivity of 0.02–0.04 mmol L^{-1} is required.

The Ca^{2+} ion probe consisted of 1,2 bis(*o*-aminophenoxy) ethane-*N*,*N*,-*N*′,*N*′-tetraacetic acid (BAPTA) moiety with a fluorophore (rhodamine). The BAPTA moiety is attached to the 9-position of rhodamine, so that the structure remains symmetrical (**Figure 4**a, Figure S2, Supporting Information). The BAPTA moiety of the sensor binds with a 1:1 stoichiometry to Ca^{2+} ions with high selectivity over Mg^{2+} ions. This is due to the design of the binding cavity, which has the suitable size for Ca^{2+} ions (ionic radius of 0.99 Å) over Mg^{2+} ions (ionic radius

© 2019 The Authors. Published by WILEY-VCH Verlag GmbH & Co. KGaA, Weinheim

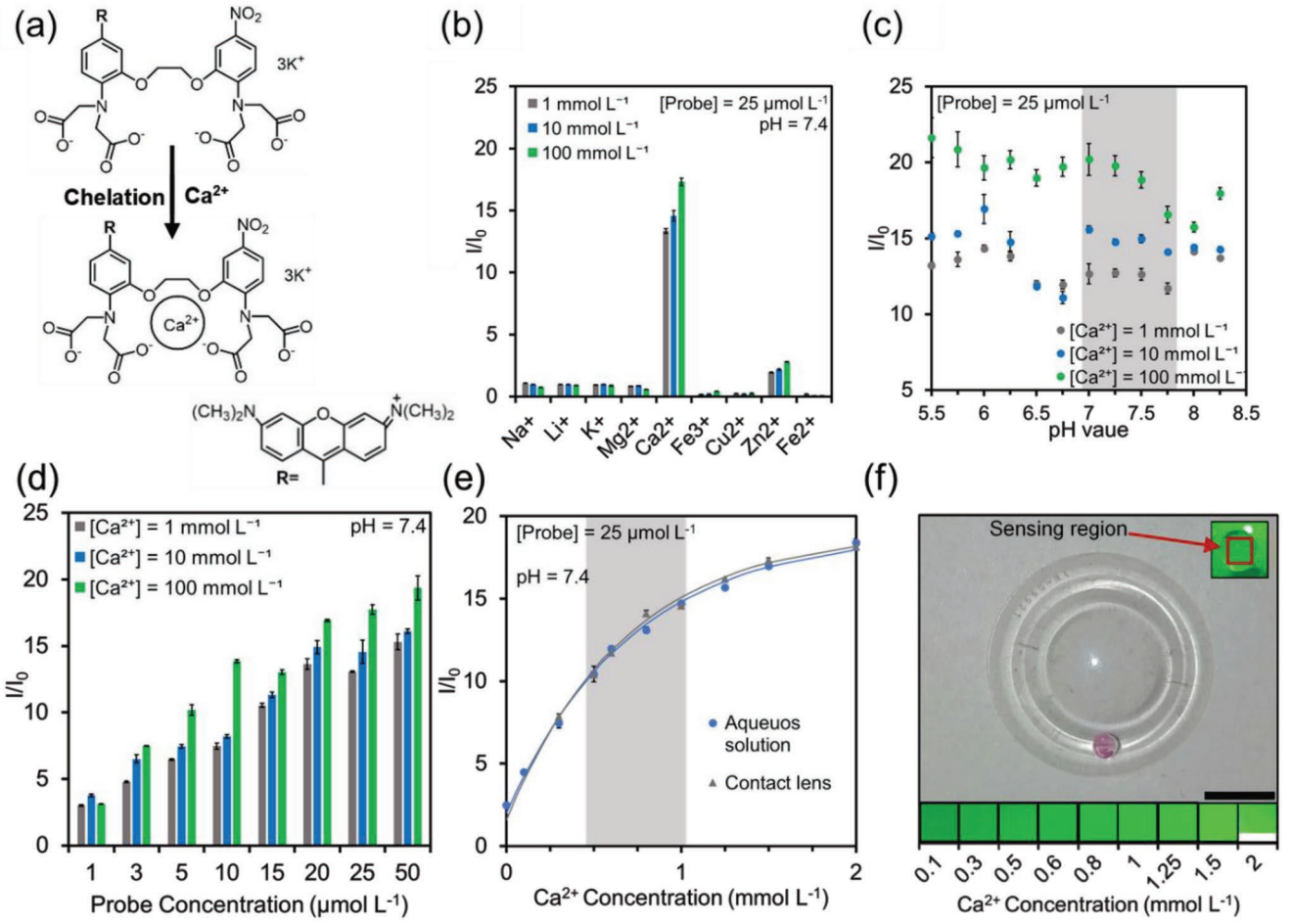


Figure 4. Quantification of Ca^{2+} ions in tris buffer solutions (pH 7.4, 150 mmol L^{-1}) with BAPTA at 24 °C. a) Chelation mechanism of BAPTA, showing a fluorescent delocalized xanthene (rhodamine) (R) and a BAPTA molecule attached to the xanthene's 9-position. The Ca^{2+} ion binds to the BAPTA moiety (1:1). b) Fluorescence readouts of BAPTA ($\lambda_{ex}/\lambda_{em}$ = 551/576 nm, 25 µmol L^{-1}) in the presence of different electrolytes (1–100 mmol L^{-1}) (n = 3). c) The effect of pH variations (pH 5.50–8.25) on BAPTA (25 µmol L^{-1}) with different Ca^{2+} ion concentrations (1–100 mmol L^{-1}) (n = 3). d) Variation of BAPTA (1–50 µmol L^{-1}) with different Ca^{2+} ion concentrations (1–100 mmol L^{-1}) (n = 3). e) Quantification of Ca^{2+} ions (0–2 mmol L^{-1}) at a constant BAPTA concentration (25 µmol L^{-1}) in aqueous solutions and scleral lens evaluated with the microplate reader and image processing algorithm (n = 3). Curves were fitted using Equation (2). f) Photograph of a scleral lens sensor with one CO_2 laser engraved concavity containing BAPTA (50 µmol L^{-1}, 2 µL). The inset shows the fluorescence emission and the sensing region in a red square (1 mm^2). Scale bar = 5 mm. Color scale of BAPTA (25 µmol L^{-1}) mixed (1:1, v/v) with Ca^{2+} ions (0.1–2.0 mmol L^{-1}) and excited with a LED (505 nm). Inset scale bar = 1 mm. Shadows in (c,e) represent the physiological range. Error bars represent the standard deviation of the mean.

of 0.65 Å).[49] The aromatic amino groups of BAPTA have a pK_a value between 5.97 and 6.36.[49]

To test the selectivity of the BAPTA to Ca^{2+} ions, the concentrations of different electrolytes were varied (1–100 mmol L^{-1}), while the concentration of BAPTA remained constant (25 µmol L^{-1}) in physiological conditions (pH 7.4). BAPTA showed the highest fluorescence intensity when bound to Ca^{2+} ions (sevenfold higher than that of Zn^{2+} ions) and the intensity increased 1.3 fold with increasing Ca^{2+} ion concentration in the solution (Figure 4b). Apart from Zn^{2+} ions, which interacted weakly with BAPTA, no other analyte had a significant response.

The response of the BAPTA to pH variation was tested. The pH of tear fluid lies between 7.14 and 7.82.[50] BAPTA (25 µmol L^{-1}) was mixed with Ca^{2+} ions (1–100 mmol L^{-1}) in tris buffer with varying pH values (pH 5.50–8.25, 150 mmol L^{-1}). The fluorescence intensity decreased by 13% overall (Figure 4c). The intensity decreased with increasing pH value and remained constant for the 1 mmol L^{-1} electrolyte solution for the physiological pH range (shadowed area). The fluorescence intensity at pH 7.75 (1 mmol L^{-1}) decreased by 7.6% as compared to the stable responses in the range of pH 7.0–7.5.

The effect of BAPTA concentration (1–50 µmol L^{-1}) on fluorescence readout was tested in different ion concentration values (1–100 mmol L^{-1}) in tris buffer (pH 7.4, 150 mmol L^{-1}) (Figure 4d). The fluorescence intensity of the probe increased 5.1-fold with increasing BAPTA concentration and 1.2-fold with increasing ionic strength. The solution containing Ca^{2+} ions (100 mmol L^{-1}) mixed with BAPTA (15 µmol L^{-1}) showed a decreased fluorescence intensity (6.2%) as compared to the same concentration mixed with 10 µmol L^{-1} BAPTA (Figure 4d).

© 2019 The Authors. Published by WILEY-VCH Verlag GmbH & Co. KGaA, Weinheim

To test the sensitivity of BAPTA (25 μmol L^{-1}) in the physiological detection range, Ca^{2+} ion solutions (0–2 mmol L^{-1}) were tested in tris buffer (pH 7.4, 150 mmol L^{-1}). Figure 4e shows the fluorescence readouts in aqueous solutions (microplate reader) and scleral lens sensor (image processing algorithm). The fluorescence intensity increased by 7.4-fold with increasing Ca^{2+} ion concentration. The dissociation constant of the BAPTA for Ca^{2+} ions was calculated to be 302 μmol L^{-1} (Equation (3)),[35,51] which was comparable with the previously reported value (320 μmol L^{-1}).[52]

Figure 4f shows a photograph of the scleral lens sensor with one laser-ablated concavity functionalized with BAPTA (2 μL, 50 μmol L^{-1}). The inset shows the LED (505 nm) excited sensor with the sensing region. The inset in Figure 4f shows the color scale of the excited BAPTA (25 μmol L^{-1}) mixed with Ca^{2+} ion solutions (0.1–2.0 mmol L^{-1}). The intensity of BAPTA increased as the Ca^{2+} ion concentration increased. BAPTA showed a high affinity for Ca^{2+} ions with a negligible interaction with Zn^{2+} ions. BAPTA exhibited a subtle pH dependency that affected the readouts with pH above 7.6 for concentrations near the physiological range (1 mmol L^{-1}). The sensitivity of BAPTA was calculated to be 0.02–0.05 mmol L^{-1} within the physiological detection range (0.50–1.25 mmol L^{-1}).

The range of Mg^{2+} ions in tear fluid lies between 0.5 and 0.9 mmol L^{-1}, where 0.61 mmol L^{-1} is the healthy concentration (Table S1, Supporting Information). Patients with MGD show a Mg^{2+} ion concentration increase of 1.6% (0.62 mmol L^{-1}), while LGD patients have 3.3% increase (0.63 mmol L^{-1}) as compared to healthy conditions. Coexistence of MGD and LGD shows the highest Mg^{2+} ion concentration with a 6.6% increase (0.65 mmol L^{-1}) in tear fluid. A Mg^{2+} ion probe that can differentiate between different subtypes of dry eye disease requires a 0.01 mmol L^{-1} sensitivity.

To measure Mg^{2+} ions, 5-oxazolecarboxylic acid (5OACA), a UV-light-excitable Mg^{2+} ion probe was selected. 5OACA is a fluorescent derivate of *o*-aminophenol-*N*,*N*,O-triacetic acid (APTRA) modified by incorporating a fluorescent aromatic group.[53] 5OACA contains a benzofuran dye (Figure S2, Supporting Information).[54] 5OACA binds with a 1:1 stoichiometry to Mg^{2+} ions (**Figure 5**a).[55] To test for the selectivity, the 5OACA (25 μmol L^{-1}) was mixed with Mg^{2+} ion solutions (1–100 mmol L^{-1}) (Figure 5b). The relative fluorescence intensity of 5OACA in response to Mg^{2+} ions (100 mmol L^{-1}, pH 7.4) was 1.9, 2.1, 1.4 folds higher than that of Na^+, K^+, Ca^{2+} ions (100 mmol L^{-1}), respectively. The relative fluorescence intensity of 5OACA (50 μmol L^{-1}) in response to Mg^{2+} ions at 10 and 1 mmol L^{-1} was 1.1 higher and 1.2 fold lower than that of Ca^{2+} ions at equivalent concentrations, respectively.

The pH influence on 5OACA was tested by using Mg^{2+} ion solutions (1–100 mmol L^{-1}) in tris buffer with varying pH values (pH 5.50–8.25, 150 mmol L^{-1}) (Figure 5c). The Mg^{2+} ion solutions were mixed (1:1, v/v) with 5OACA (25 μmol L^{-1}). In acidic and basic conditions, the fluorescence intensity showed a constant increase with increasing pH value (1.9-fold increased intensity from pH 5.50 to 8.25). Within the physiological pH range, 5OACA had an almost stable response, a subtle fluorescence intensity increase (8%) was measured between pH 7.0 and 7.8. The concentration of the 5OACA was varied (1–50 μmol L^{-1}) to test the Mg^{2+} ions with different concentrations (1–100 mmol L^{-1}) (Figure 5d). The fluorescence intensity increased 1.2-fold with increasing 5OACA concentration and 2.4-fold with increasing Mg^{2+} ion concentration.

Mg^{2+} ion solutions with varying ionic strengths (0–2 mmol L^{-1}) were prepared in tris buffer (pH 7.4, 150 mmol L^{-1}) and mixed (1:1, v/v) with 5OACA (25 μmol L^{-1}). The fluorescence intensity increased 5.4 fold with increasing Mg^{2+} ion concentrations, and a 1.2 fold increase within the physiological detection range using the microplate reader, where the results were comparable with the measurements in a scleral lens sensor using an image processing algorithm (Figure 5e). 5OACA (1 μL, 25 μmol L^{-1}) and Mg^{2+} ion solutions (1 μL, 0.3–2.0 mmol L^{-1}) were immobilized in the scleral lens and excited with a LED (340 nm). The dissociation constant for 5OACA was calculated to be 2.1 mmol L^{-1}, which was in contrast to the reported K_d value (1.5 mmol L^{-1}).[56] Figure 5f shows 5OACA (2 μL, 50 μmol L^{-1}) immobilized in the scleral lens concavity. The fluorescence intensity of 5OACA increased with increasing Mg^{2+} ion concentration (0.1–2.0 mmol L^{-1}). The 5OACA (25 μmol L^{-1}) mixed with Mg^{2+} ions was excited with a 340 nm LED and photographs were taken through a 500 nm bandpass filter, and it exhibited a subtle pH dependency in the entire physiological pH range. The sensitivity of the probe was calculated to be 0.01–0.03 mmol L^{-1} within the physiological range, suitable for differentiating between dry eye subtypes.

Zn^{2+} ions are important for the immune system and are needed for the stabilization of nucleic acids, cell membranes, and cellular organelles.[57] Low Zn^{2+} ion concentration prolongs the corneal repair process, affecting the ocular physiology and cell function that could lead to night blindness and blurred vision.[58,59] The fluorescent *N*-(2-methoxyphenyl) iminodiacetate (MPIDA) was chosen as the Zn^{2+} ion sensor. MPIDA consists of a xanthene linked to a chelation site,[54] which binds Zn^{2+} ion with 1:1 stoichiometry (**Figure 6**a).[60] The fluorescence is due to a photoinduced electron transfer (PET) switching mechanism, where the xanthene's fluorescence is quenched by the chelation moiety (Figure S2, Supporting Information).[61] The anilinyl chelation moiety[61] of the Zn^{2+} ion sensor is a modified BAPTA chelator.[57] Upon binding Zn^{2+} ions (100 μmol L^{-1}), the fluorescence intensity of MPIDA increases.[57] To test the selectivity of the sensor, MPIDA (25 μmol L^{-1}) was mixed with different electrolytes (1–100 mmol L^{-1}) in tris buffer (pH 7.4, 150 mmol L^{-1}). MPIDA showed the highest interaction upon binding Zn^{2+} ions, increasing its fluorescence intensity 1.5-fold with increasing Zn^{2+} ion concentrations (Figure 6b).

The effect of pH variance on fluorescence readouts was tested while the MPIDA concentration remained constant (25 μmol L^{-1}). Zn^{2+} ions were prepared in tris buffer solution with varying pH values (pH 5.50–8.25, 150 mmol L^{-1}) and mixed (1:1, v/v) with MPIDA. In extreme acidic and basic conditions, there was a varying response for MPIDA; however, within the physiological pH range, the probe exhibited a stable fluorescence intensity for all the solutions (Figure 6c).

The effect of variation in MPIDA concentration in sensing Zn^{2+} ions was tested. MPIDA at different concentrations (1–50 μmol L^{-1}) was mixed (1:1, v/v) with Zn^{2+} ion solutions (1–100 mmol L^{-1}) were prepared in tris buffer (pH 7.4, 150 mmol L^{-1}). The fluorescence intensity increased 7-fold with

© 2019 The Authors. Published by WILEY-VCH Verlag GmbH & Co. KGaA, Weinheim

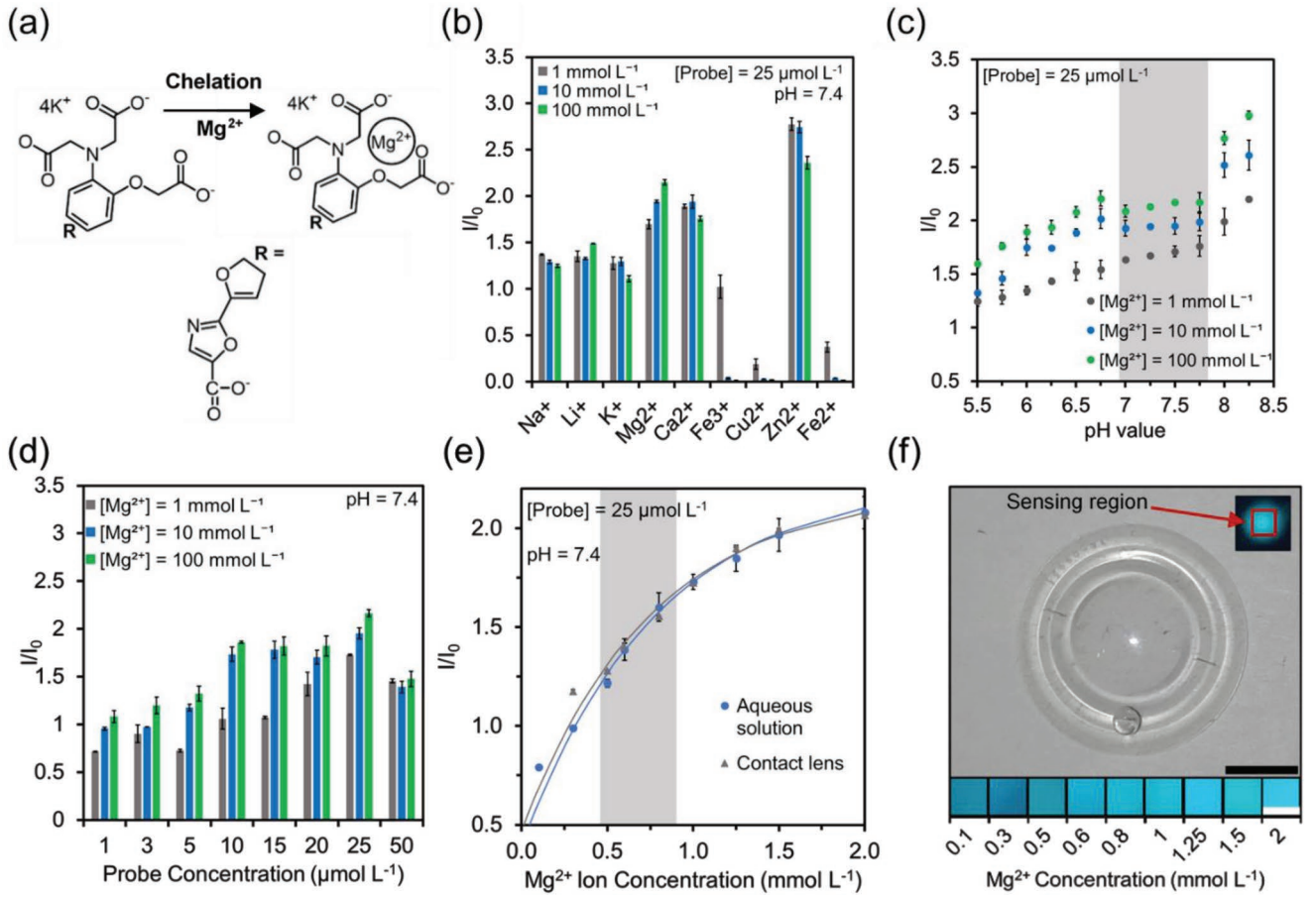


Figure 5. Quantification of Mg^{2+} ions in tris buffer solutions (pH 7.4, 150 mmol L^{-1}) with 5OACA at 24 °C. a) Chelation mechanism of 5OACA. Furan fluorophore (R) linked to an APTRA moiety. APTRA chelator bound 1:1 to the Mg^{2+} ion. b) Fluorescence readouts of 5OACA ($\lambda_{ex}/\lambda_{em}$ = 330/510 nm) (25 µmol L^{-1}) in the presence of different electrolytes (1–100 mmol L^{-1}) (n = 3). c) The effect of pH variation (pH 5.50–8.25) on 5OACA (25 µmol L^{-1}) with varying Mg^{2+} ions (1–100 mmol L^{-1}) (n = 3). d) Variation of 5OACA concentration (1–50 µmol L^{-1}) in different Mg^{2+} ion concentrations (1–100 mmol L^{-1}) (n = 3). e) Quantification of Mg^{2+} ions (0–2 mmol L^{-1}) in 5OACA (25 µmol L^{-1}) (n = 3). Blue dots show the microplate readouts, gray dots show the scleral lens with varying Mg^{2+} ion concentrations (0.3–2.0 mmol L^{-1}). The curves show the fitted data for Mg^{2+} ion quantification with Equation (2). f) Photograph of an engraved scleral lens with one concavity containing 5OACA (50 µmol L^{-1}, 2 µL). Scale bar = 5 mm. Inset shows the fluorescence emission and the sensing region in a red square (1 mm^2). The inset scale bar shows fluorescence intensity increase with increasing Mg^{2+} ion concentration (0.1–2.0 mmol L^{-1}), 5OACA (25 µmol L^{-1}). A 340 nm LED was used to excite the sensor and a 500 nm bandpass optical filter (FWHM = 40 ± 8 nm) allowed filtering out the emission. Inset scale bar = 1 mm. Shadowed areas in Figure 3c,e show the physiological ranges. Error bars represent the standard deviation of the mean.

increasing MPIDA, as well as 1.2-fold for increasing Zn^{2+} ion concentration (Figure 6d).

The sensitivity of MPIDA (25 µmol L^{-1}) to Zn^{2+} ions (0–50 µmol L^{-1}) was tested in tris buffer (pH 7.4, 150 mmol L^{-1}) (Figure 6e). The fluorescence intensity of MPIDA showed a 2.6-fold increase with increasing Zn^{2+} ion concentration, comparable to the data in the scleral lens concavity. The dissociation constant of Zn^{2+} ions for MPIDA was calculated to be 16 µmol L^{-1} (Equation (3)), contrasting the previously reported value (7.8 µmol L^{-1}).[57,61] Figure 6f shows a scleral lens sensor with an engraved concavity functionalized with MPIDA (2 µL, 50 µmol L^{-1}). The inset in Figure 6f shows the sensing region of the sensor. The color scale showed the fluorescence intensity of MPIDA increasing with increasing Zn^{2+} ion concentration (10–50 µmol L^{-1}). MPIDA (1 µL, 25 µmol L^{-1}) was mixed with Zn^{2+} ion concentrations (1 µL) and in the scleral lens concavity. The MPIDA in the scleral lens was excited using a 555 nm LED and filtered by a 580 nm bandpass filter. The MPIDA probe showed high selectivity for Zn^{2+} ions and a pH invariance within the physiological pH range. The sensitivity of MPIDA was calculated to be 1 µmol L^{-1} using Equation (3), which is suitable to measure Zn^{2+} ions in physiological conditions.

To create enclosed sensing regions and multiplex the probes, the scleral lens was sealed with a silicone hydrogel membrane (30 µm, midafilcon). The enclosed channels prevented the leakage of fluorophores from the sensing regions while allowing the diffusion of electrolytes into the sensing regions. **Figure 7**a illustrates a scleral lens with enclosed microchannels as rhodamine B solution (10 mmol L^{-1}) was injected using a syringe pump (1 µL min^{-1}). Further injection of the fluid into the scleral lens demonstrated that the scleral lens was sealed completely and no fluorophore dye leakage was observed (Figure 7b). Figure 7c demonstrates a scleral lens with multiplexed sensing regions. Figure 7d shows the fluid flow

© 2019 The Authors. Published by WILEY-VCH Verlag GmbH & Co. KGaA, Weinheim

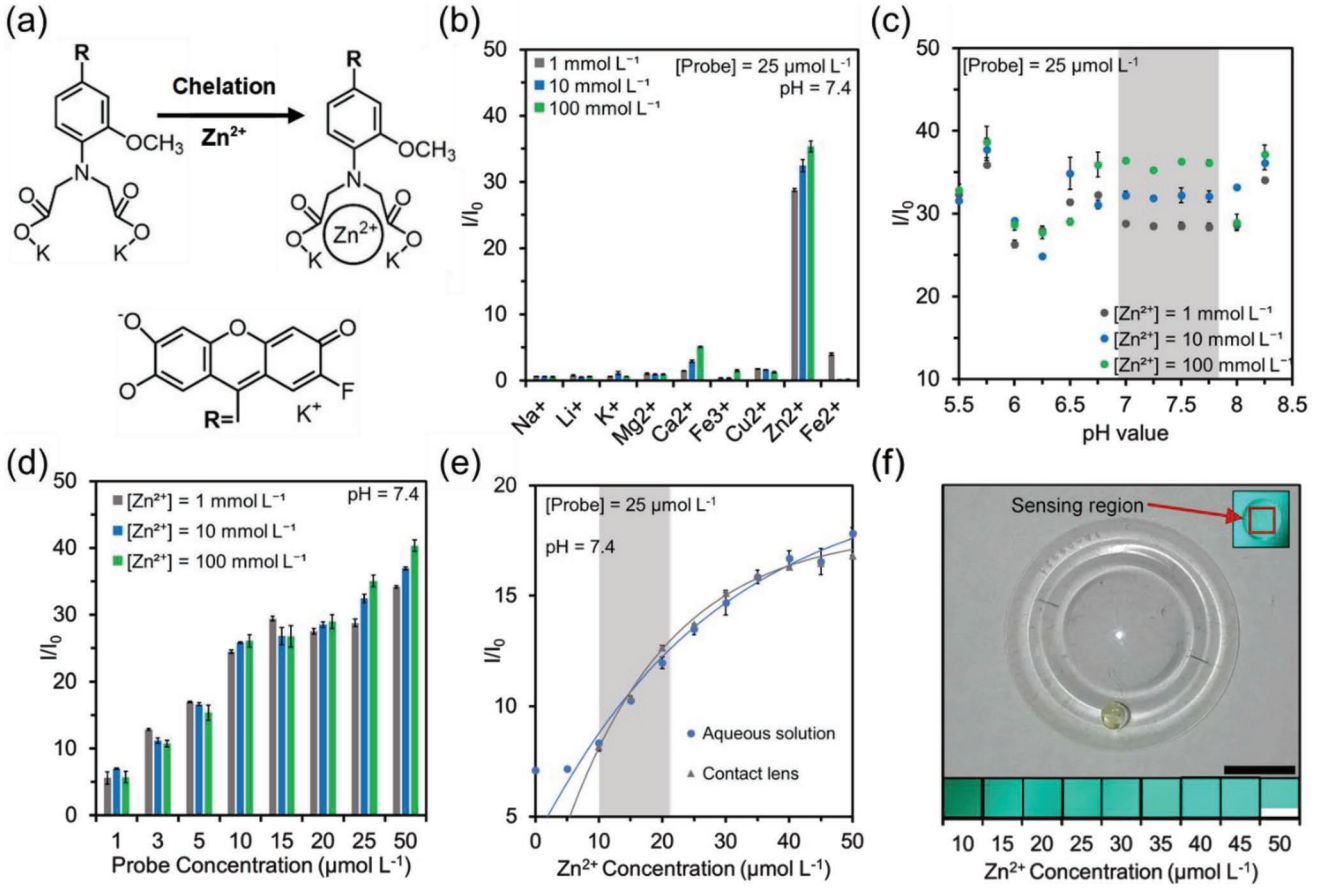


Figure 6. Quantification of Zn^{2+} ions in tris buffer solutions (pH 7.4, 150 mmol L^{-1}) with MPIDA at 24 °C. a) Chelation mechanism of MPIDA: a modified BAPTA moiety is bound to a fluorescent reporter (R). The chelation site binds (1:1) to a Zn^{2+} ion. b) Fluorescence readouts of MPIDA ($\lambda_{ex}/\lambda_{em}$ = 551/576 nm) (25 µmol L^{-1}) in the presence of different ions (1–100 mmol L^{-1}) (n = 3). c) The effect of pH variations (pH 5.50–8.25) on MPIDA (25 µmol L^{-1}) at varying Zn^{2+} ion concentrations (1–100 mmol L^{-1}) (n = 3). d) Variation of MPIDA concentration (1–50 µmol L^{-1}) with varying Zn^{2+} ion concentration (1–100 mmol L^{-1}) (n = 3). e) Quantification of Zn^{2+} ions (0–50 µmol L^{-1}) at constant MPIDA concentration (25 µmol L^{-1}) (n = 3) in aqueous solutions using a microplate reader and in the scleral lens sensor using the image processing algorithm (n = 3). Data fitted with Equation (2). f) Photograph of a scleral lens with one CO_2 laser engraved concavity and MPIDA (50 µmol L^{-1}). Scale bar = 5 mm. Inset shows the fluorescence emission and the sensing region (1 mm^2). Intensity scale of MPIDA (25 µmol L^{-1}) mixed (1:1, v/v) with Zn^{2+} ion concentrations (10–50 µmol L^{-1}). Excitation with a 555 nm LED, the photograph was taken through a 580 nm bandpass optical filter (FWHM = 10 ± 2 nm). Inset scale bar = 1 mm. Shadows in (c,e) show the physiological range. Error bars represent standard deviation of the mean.

of artificial tear fluid in the microchannels of a fully enclosed scleral lens having branching channels and a mixer. Figure 7e shows brightfield and fluorescence images of the multiplexed scleral lens sensors with ablated concavities (Ø = 1.5 mm). The scleral lens sensor was excited using the readout device with the LED (340 nm) in the readout device and the emitted light was filtered out. The brightest spot was the UV-excitable 5OACA. Multiplexing the sensors did not cause a cross-talk as the sensors are physically separated and the weak fluorescence does not interfere with the measurements, demonstrating the feasibility of multiplexing the probes in a single scleral lens sensor.

For point-of-care diagnostics, a portable readout device was developed to create a stable and consistent lightning condition (**Figure 8**a). The device was designed to read a multiplexed scleral lens sensor. The circular sensor excitation site consisted of three LEDs with 340, 505, and 555 nm emission wavelengths, respectively. The device contained three changeable lids that are integrated with bandpass filters of 500, 530, and 580 nm to transmit the emission wavelengths of the sensors (Figure 8b). The device had a circular sensing site that fitted over the eye socket (Figure 8c). Thus, the probes multiplexed on the scleral lens sensor could be excited directly on the eye. The chamber on the bottom of the device held the battery for easy access. The user could switch on the appropriate LED and use the bandpass filter according to the electrolyte type. The optical response of the ion sensors on the scleral lens was captured by a smartphone camera through an optical filter.

A smartphone algorithm and an interface were developed to provide quantitative results from scleral lens sensors. The captured photographs are processed by the readout algorithm integrated into a smartphone application, which calculates the mean gray value and standard error of the images. The data are used to correlate the ion concentration of the analyzed sensor by referring to the previously stored relative fluorescence intensity curves of electrolytes with different ionic strengths. The code subsequently returns concentrations for multiple analytes to provide

© 2019 The Authors. Published by WILEY-VCH Verlag GmbH & Co. KGaA, Weinheim

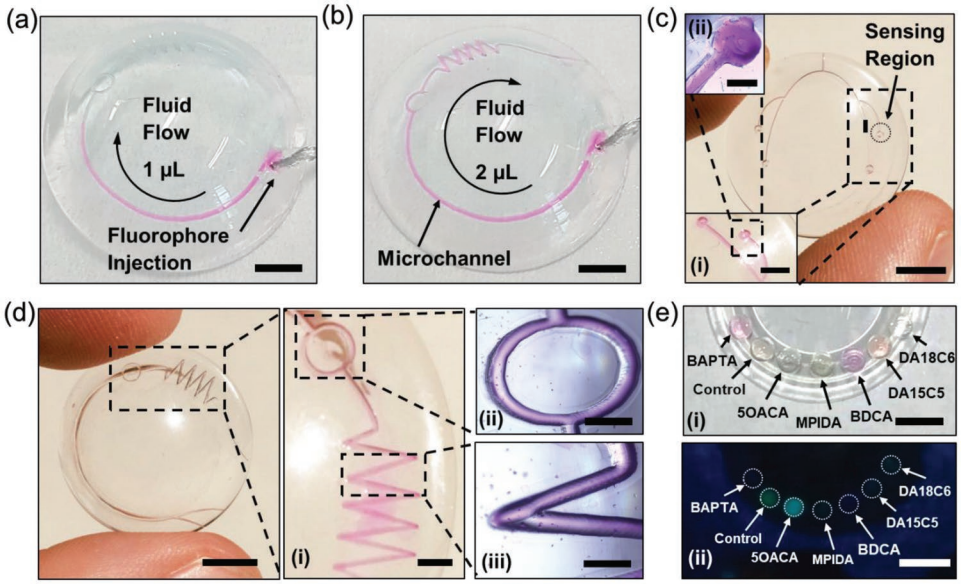


Figure 7. Multiplexed scleral lens for dry eye severity and subtype diagnosis in artificial tear fluid. a) Photograph of the scleral sensors consisting of a silicone hydrogel seal (30 µm, midafilcon, showing the fluid flow (1 µL, rhodamine B, 10 mmol L^{-1}) in an enclosed microchannel. Scale bar = 5 mm. b) Fluid flow (2 µL) progress within the close microchannel system. Scale bar = 5 mm. c) Photograph of a scleral lens having a multiplexed microchannels and sensing regions. Scale bar = 5 mm. The insets show: i) the branching sensing regions (scale bar = 3.0 mm) and ii) a magnified sensing region (scale bar = 500 µm). d) Photograph of the microchannel in the scleral lens having branching channels and a mixer. The insets show: i) the mixer and branching microchannels (scale bar = 1.0 mm), ii) a magnified branching microchannel (scale bar = 500 µm), and iii) a magnified mixer (scale bar = 500 µm). e) Photographs of a multiplexed scleral lens with fluorescent probes (50 µmol L^{-1}) to measure pH, Na^+, K^+, Ca^{2+}, Mg^{2+}, and Zn^{2+} ions. i) Brightfield image and ii) fluorescence image under LED excitation (340 nm). Scale bars = 5 mm.

a diagnostic result. The first step that the algorithm performs is the calibration of the data. Known curves of the concentration-dependent relative fluorescence increase are input to the algorithm. These curves correspond to the fitted data points obtained from laboratory electrolyte solutions. After loading the curves, calibration points near the physiological range of each analyte are chosen. The mathematical calibration intensity is calculated with the fitted data curve, which returns the intensity value obtained from the characterization experiments. Then, the customized function image analysis is called. Its input values are three images of the same excited electrolyte sensor at known concentrations. This function analyses the images by calculating the mean intensity of the input pictures (1 mm^2). In the picture matrix, the image is converted to grayscale and the algorithm saves it as a 2D matrix in the workspace. The algorithm sums all the elements of the gray-scaled matrix and divides them by the number of elements to obtain the average intensity of the image. This procedure is repeated for the two remaining images. The image analysis function returns the mean intensity of the images and the standard deviation of the mean. To make the calculated image intensity comparable to the reference data obtained by the experiments, the mathematical intensity point is divided by the mean intensity obtained by the image analysis function. The obtained number (calibration multiplier) allows comparing the intensity values determined by the algorithm to the experimental intensity values. After the mean intensity of the image is calculated, and if the sensor does not show pH dependency, the calculated intensity value is multiplied by the previously determined calibration multiplier to obtain the normalized intensity, which is comparable to the reference data given by

$$C = \frac{\log\left(1 - \frac{I'(C)}{I'_s}\right)}{-\infty} - a \tag{4}$$

Inserting the normalized intensity for $I'(C)$ in Equation (4) returns the unknown concentration C. For the determination of the pH value, the Henderson–Hasselbalch equation was used. In case the sensor shows pH dependency, an additional value is multiplied with the normalized intensity before inserting it in Equation (4). This value was determined from the pH invariance characterization experiments. The pH deconvolution occurs within the pH deconvolution function, which serves as a database of the sensors' exhibited pH dependencies. The function is called with the analyte to be measured, the pH value, and the current calculated intensity. The output value is the corrected normalized intensity. The interaction of the sensor with other electrolytes can also be deconvoluted by the algorithm. The ion deconvolution function allows for deconvoluting ion interference. Analogous to the pH deconvolution function, the input arguments are the analyte to be measured, the concentration of the interfering electrolyte, and the current calculated intensity. The ion deconvolution function returns the corrected normalized intensity value that is used for further ion value corrections. A database was generated for the deconvolution of ion interference (Figure S3, Supporting Information). For example, deconvolution experiments were performed on the Mg^{2+} ion sensor. Ca^{2+} ions (0.50–1.25 mmol L^{-1}) and Zn^{2+} ions (10–20 µmol L^{-1}) were mixed (1:1, v/v) with the 5OACA (25 µmol L^{-1}) to obtain the necessary deconvolution data for the algorithm. The deconvolution experiments performed with

© 2019 The Authors. Published by WILEY-VCH Verlag GmbH & Co. KGaA, Weinheim

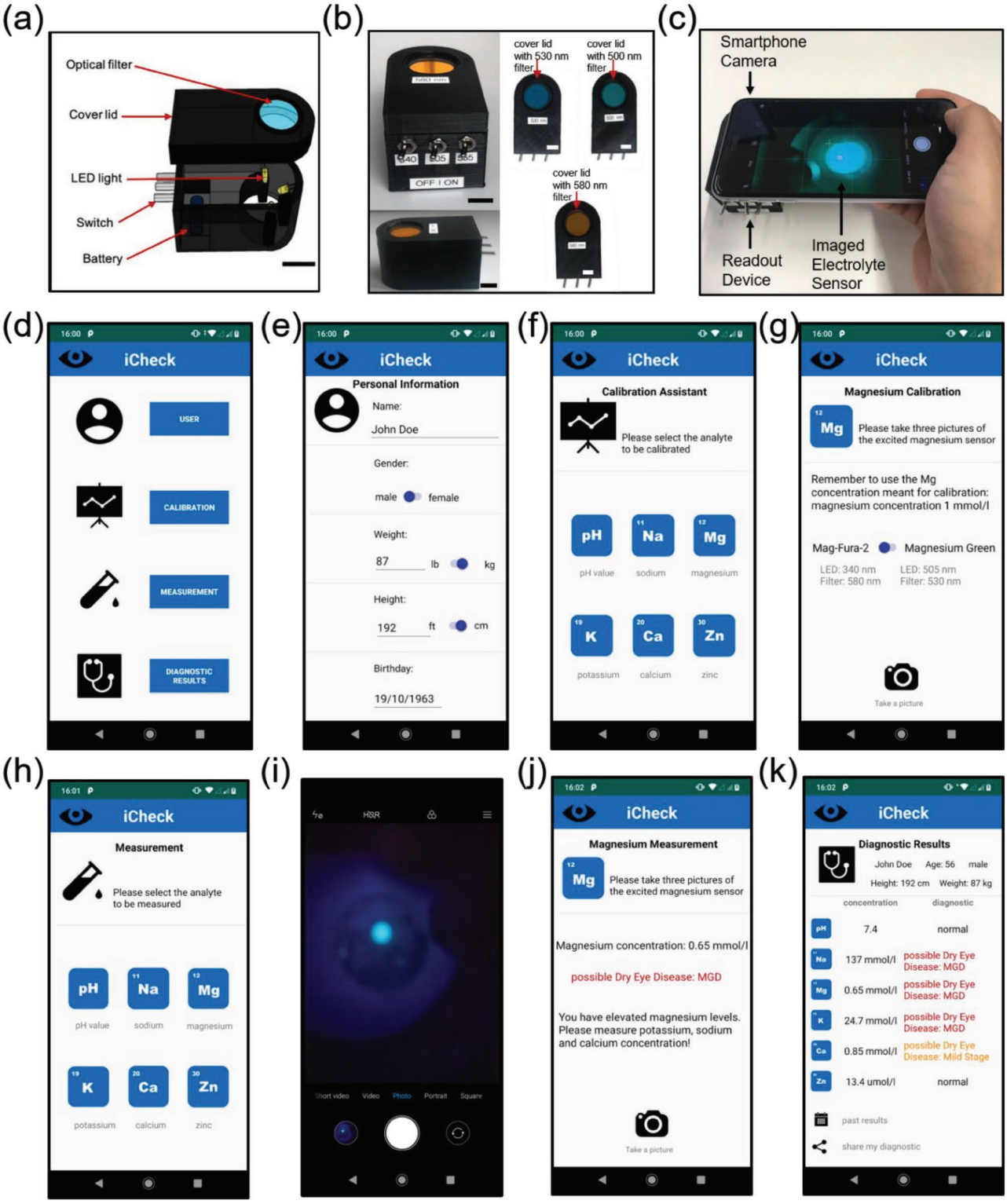


Figure 8. Readout device interfaced with a smartphone for tear electrolyte analysis. a) The device for fluorescence excitation and exchangeable bandpass filters. Scale bar = 1 cm. b) The readout device with changeable bandpass filters. Scale bar = 2 cm. c) Demonstration of the portable readout device over the eye socket for exciting and capturing the images of the fluorescent probes. Scale bar = 2 cm. d) User interface of the smartphone application: home screen. e) User window to enter patient information. f) Calibration assistant screen to select the analyte to be calibrated. g) The user can indicate the sensor type. h) Measurement screen to select the analyte to be measured. i) Camera access through the application taking a picture of the LED-excited (340 nm) sensor. j) The measurement of an electrolyte. After performing the measurement, a diagnostic result is displayed. k) Diagnostic results screen, showing an overview of the performed measurements.

© 2019 The Authors. Published by WILEY-VCH Verlag GmbH & Co. KGaA, Weinheim

5OACA showed a stable response for Ca^{2+} ions within the physiological range (Figure S3, Supporting Information). In the case of Zn^{2+} ion deconvolution, the fluorescence intensity increased 1.3-fold with increasing Zn^{2+} ion concentration in the solution. The Ca^{2+} ion interference was deconvoluted as a constant, non-concentration dependent offset. Therefore, only Zn^{2+} ion concentration needed to be known before measuring Mg^{2+} ion concentration. If the user attempted to measure Mg^{2+} ions, the algorithm checked whether Zn^{2+} ion had been measured. If Zn^{2+} ion concentration was still unknown, the algorithm requested the user to measure Zn^{2+} ions first before proceeding to measure Mg^{2+} ions. After measuring the selected analyte, the algorithm outputs a diagnosis overview displaying the determined concentration and a warning if the analyte is not within healthy concentration range, pointing out the severity stage of dry eye and its subtype.

To make the measurements of electrolytes in tear fluid more intuitive and user-friendly, the prototype of a user interface for a smartphone application iCheck was designed in Android Studio. Figure 8d shows the home screen of the application. In user screen, the patient information can be entered to record the patient data and measurements (Figure 8e). In calibration, the calibration of the selected analyte was performed (Figure 8f). Selecting the analyte opens a new tab, where the user can select the reference data for precalibrated fluorescent probes or the user can take photographs of the reference images with known concentrations to perform the calibration (Figure 8g). LED and filter types are also displayed in this screen. Measurement allows choosing an analyte to perform the measurement (Figure 8h). Selecting an analyte grants the application access to the camera to take the pictures of the LED-excited sensor with the unknown electrolyte concentration (Figure 8i). The application displays the measurement results (Figure 8j). In the last step, under the diagnostic results button, a summary of the performed measurements and a possible diagnosis are displayed (Figure 8k). Furthermore, the user has the option to view past measurements under the calendar button or share the information.

To test the sensitivity of the developed sensing system in dry eye diagnostics, artificial tear fluid analysis was performed. Artificial tear fluid containing H^+, Na^+, K^+, Ca^{2+}, Mg^{2+}, Zn^{2+} ions and other biological tear constituents to mimic the composition of human tears with MGD, LGD, and MGD/LGD (Table S2, Supporting Information). Each artificial tear fluid was mixed (1:1, v/v) with the fluorescent probes (50 µmol L^{-1}, 4 µL) in the concavity on the scleral lens sensor. Photographs of the electrolyte sensors were captured with a smartphone camera and input to the algorithm to estimate the concentration of the electrolytes. **Figure 9** shows the results of the artificial tear fluid analysis in dry eye diagnosis. Evaluated probes with the readout system provided data for diagnosing the severity and the subtype differentiation of the dry eye syndrome. The obtained results were deconvoluted to approximate the true values. For example, after artificial tear fluid was added to 5OACA, the concentration of Mg^{2+} ions was deconvoluted based on pH, Ca^{2+}, and Zn^{2+} ions.

Both BDCA and DA18C6 were sensitive in the detection range and did not interact with other analytes. However, the sensitivity of DA15C5 was limited within the physiological range. One approach to solve this problem could be to use a microfluidic dilution component in the scleral lens concavity.[41] Another approach could be to use a Na^+ ion probe with higher K_d values (80 mmol L^{-1}).[62] The selectivity of the 5OACA[53] can be increased by modified APTRA moieties using phosphinate-based chelators to measure Mg^{2+} ions selectively over Ca^{2+} ions.[63] The acute and chronic oral toxicities of 15-crown-5 and 18-crown-6 have been studied in mice.[64] The median lethal dose (LD50) values were determined to be 1.02 g kg^{-1} (15-crown-5) and 0.71 g kg^{-1} (18-crown-6). Increase in crown ether ring size and water solubility increases toxicity. Another study of crown ethers in Chinese hamster V79 cells has shown no genotoxic effect in mammalian cells.[65] However, the toxicological properties of crown ethers have not been fully investigated in the eye; and therefore, crown ethers should be covalently linked to the scleral lens matrix through acryloyl groups to prevent leaching over the ocular surface. Furthermore, the fluorescent probes described in the present work are temperature sensitive; however, the ocular surface temperature is tightly regulated within 28–33 °C. Hence, having a temperature calibration could compensate for the measurement errors. Additionally, the shelf life of the probes should be evaluated to determine the stability at room temperature.

In the readout device, specular reflection on the scleral lens sensor could be eliminated by adopting an optical diffuser. A low-intensity UV-LED was used to excite DA18C6; however, the health effects of exposure to UV light sources on the human eye must be considered.[66] Additionally, automated optical filter and LED system shutter control could eliminate the requirement of cover lids for each optical filter and the time to switch the LEDs on/off to reduce the measurement time. Furthermore, spectral peak changes based on red-green-blue (RGB) can be used as a secondary data set to supplement fluorescence intensity measurements to increase the readout accuracy.[67]

The quantification of electrolytes in tear fluid offers possibilities for diagnosing multiple ocular diseases or systemic disorders. A shift in the ocular surface pH not only is an indicator for the dry eye disease, but also can be a sign of rosacea, allergenic reactions, and bacterial infections.[68] Furthermore, children with cystic fibrosis demonstrated a difference in Na^+ ion concentration of tear fluid.[69] Additionally, higher Ca^{2+} ion concentrations in tear fluid of children can indicate cystic fibrosis.[69] K^+ ions play a role in the maintenance of corneal thickness and that K^+ ion deficiency in the tear film leads to corneal swelling.[70] Ca^{2+} and Mg^{2+} ion quantification in tears have the potential to determine hypo- or hypercalcemia.[71] Additionally, Zn^{2+} ion deficiency can promote cataractogenesis.[59] Hence, the measurement of tear electrolytes have broader diagnostic potential beyond dry eye syndrome.

The scleral lens sensor allowed quantitatively measuring the fluorescence emission of pH and electrolytes to assess the tear film in point-of-care settings. Quantifying the electrolytes in the human tear fluid enables differentiation between the MGD and LGD subtypes of the dry eye syndrome in 5 min. An advantage of the scleral lens sensor is that it is power free, which eliminates the negative health effects of electromagnetic radiation of wireless powering. The scleral lens sensor relies only on optical measurement and does not require any built-in

© 2019 The Authors. Published by WILEY-VCH Verlag GmbH & Co. KGaA, Weinheim

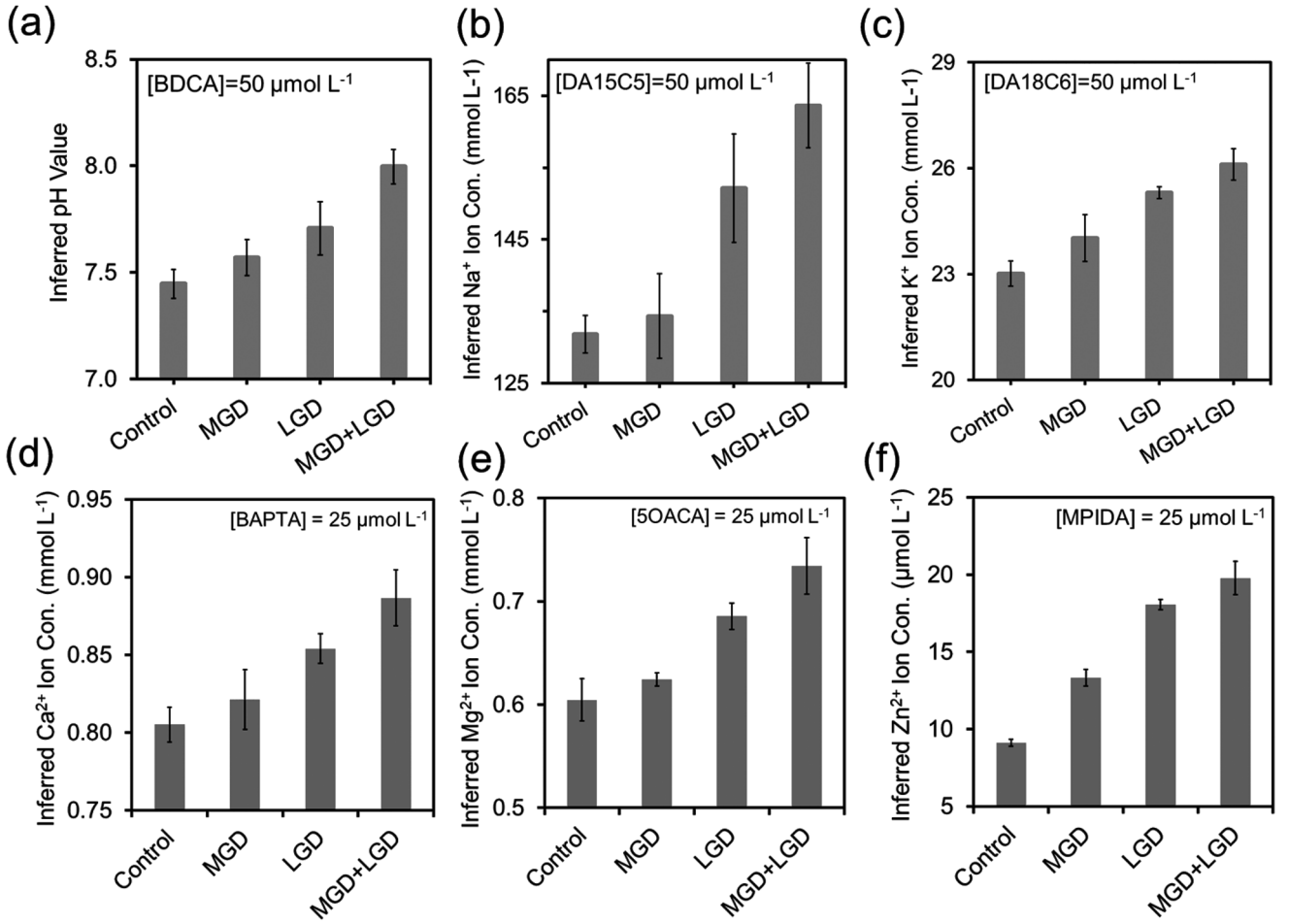


Figure 9. Measurements of electrolytes in a multiplexed scleral lens for dry eye severity and subtype diagnosis in artificial tear fluid using a smartphone. a) Inferred pH values in BDCA (50 μmol L^{-1}) (n = 3). b) Inferred Na^+ ion concentrations in DA15C5 (50 μmol L^{-1}) (n = 3). c) K^+ ions in DA18C6 (50 μmol L^{-1}) (n = 3). d) Inferred Ca^{2+} ion concentration containing BAPTA (25 μmol L^{-1}) (n = 3). e) Inferred Mg^{2+} concentration with 5OACA (25 μmol L^{-1}) (n = 3). f) Inferred Zn^{2+} ion concentration (25 μmol L^{-1}) in MPIDA (25 μmol L^{-1}) (n = 3). Error bars represent the standard error the mean.

electronics, which immensely simplifies its working principle and facilitates its clinical utility.

Experimental Section

Materials: All chemicals were of analytical grade and used without further purification. The following chemicals were purchased from Fisher Scientific: tris base (≥99.8%), tris hydrochloride (tris HCl, 99%) sodium chloride (NaCl) (≥99.5%), potassium chloride (KCl) (>99%), magnesium chloride (MCl_2) (≥98.0%), calcium chloride dihydrate ($CaCl_2{\cdot}2H_2O$) (>99%), iron(III) chloride hexahydrate ($FeCl_3{\cdot}6H_2O$) (>99%), copper(II) chloride dihydrate ($CuCl_2{\cdot}2H_2O$) (99%), nickel(II) sulfate hexahydrate ($NiSO_4{\cdot}6H_2O$) (99%), zinc chloride ($ZnCl_2$) (>97%), lithium chloride (LiCl) (≥99%), iron(II) chloride tetrahydrate ($FeCl_2{\cdot}4H_2O$) (98%), dimethyl sulfoxide (DMSO) (%99.9), benzenedicarboxylic acid, 2(or 4)-[10-(dimethylamino)-3-oxo-3*H*-benzo[c]xanthene-7-yl]- 126208−12-6 (HPLC purity ≥95%, $\lambda_{ex}/\lambda_{em}$:520/590 nm), tetra(tetramethylammonium) salt (HPLC purity ≥90%, $\lambda_{ex}/\lambda_{em}$:492/520 nm), 1,3-benzenedicarboxylic acid, 4,4′-[1,4,10,13-tetraoxa-7,16-diazacyclooctadecane-7,16-diylbis (5-methoxy-6,2-benzofurandiyl)]bis(tetraammonium salt) (HPLC purity ≥90%, $\lambda_{ex}/\lambda_{em}$:340/505 nm), Rhod-5N (tripotassium salt, cell impermanent) ($C_{39}H_{36}K_3N_5O_{13}$) ($\lambda_{ex}/\lambda_{em}$ = 551/576 nm), magnesium green (pentapotassium salt, cell impermanent) ($C_{33}H_{17}Cl_2K_5N_2O_{13}$) ($\lambda_{ex}/\lambda_{em}$ = 506/531 nm), Mag-Fura-2 (tetrapotassium salt, cell impermanent) ($C_{18}H_{10}K_4N_2O_{11}$) ($\lambda_{ex}/\lambda_{em}$ = 330/505 nm), FluoZin-1 (tripotassium salt, cell impermanent) ($C_{24}H_{14}F_2NO_8K_3$) ($\lambda_{ex}/\lambda_{em}$ = 495/515 nm). Scleral lenses (paflufocon; SPH: multiple; DIA 15.00–18.00 mm; BC: multiple) were provided by Falco Linsen AG (Switzerland).

Equipment: Microplate reader (FLUOstar Galaxy from BMG Labtechnologies, Software Version: 4.31-0, Firmware Version 4.31-0) was used to assess the fluorescence intensity of the prepared 96-well plate assays. A lab pH meter inoLab pH 7110 was used to prepare the solutions with varying pH values. The UV–vis-spectrometer Specord 250 from Analytik lena was used to take the UV–vis spectroscopy of the sensors and the obtained spectral data were analyzed with the Software WinAspect. For the fabrication of the readout device 340, 505, and 555 nm LEDs; together with 530 nm (FWHM = 10 ± 2 nm), 580 nm (FWHM = 10 ± 2 nm), and 500 nm (FWHM = 40 ± 8 nm) bandpass filters were purchased from ThorLabs. A Xiaomi Mi A2 Lite (Android 9, API 28) was used to capture the images that were later used as an input for the readout algorithm and to test the application that was developed in Android Studio. The algorithm was developed in MATLAB R2018b.

Preparation of Ion Solutions: 7.26 g of tris base and 9.46 g of Tris-HCl powder were each diluted in 400 mL of deionized (DI) water. While

© 2019 The Authors. Published by WILEY-VCH Verlag GmbH & Co. KGaA, Weinheim

monitoring with an electrochemical pH meter, these two stock solutions were mixed to obtain Tris buffer solutions with pH values ranging from pH 4.0 to 9.0 with a constant ionic strength (150 mmol L^{-1}). NaCl (0.292 g), LiCl (0.212 g), KCl (0.373 g), $MgCl_2$ (0.476 g), $CaCl_2 \cdot 2H_2O$ (0.735 g), $FeCl_3 \cdot 6H_2O$ (1.351 g), $CuCl_2 \cdot 2H_2O$ (0.852 g), $ZnCl_2$ (0.681 g), $NiSO_4 \cdot 6H_2O$ (1.314 g), and $FeCl_2 \cdot 4H_2O$ (0.994 g) were mixed with 25 mL Tris buffer solution (pH 4.0–9.0, 150 mmol L^{-1}) to obtain 200 mmol L^{-1} ion concentration stock solutions. The stock solutions were further diluted to obtain the necessary concentrations for all experiments.

Preparation of Artificial Tear Fluid: Artificial tear fluid was simulated by mixing relevant ions contained in tear fluid and adding 0.05 mmol L^{-1} of glucose. Different disease stages of dry eye were simulated by preparing artificial tear fluid (Tables S2 and S3, Supporting Information).

Preparation of Fluorescent Probes: Fluorescent probes were prepared to obtain 1 mmol L^{-1} stock solutions. Stock solutions of 1 mmol L^{-1} containing 1 mg BDCA (MW: 453.45 g mol^{-1}), 1 mg DA15C5 derivative (MW: 1667.57 g mol^{-1}), and 1 mg DA18C6 derivative (MW: 950.99 g mol^{-1} were prepared in 2205, 600, and 1052 µL DI water respectively. The Ca^{2+} ion probe Rhod-5N tripotassium salt (500 µg, MW: 900.034 g mol^{-1}) was prepared in 556 µL distilled water. Magnesium green pentapotassium salt (1 mg, MW: 915.9004 g mol^{-1}) was dissolved in 1092 µL distilled water. To Mag-Fura-2 tetrapotassium salt (1 mg, MW: 586.68 g mol^{-1}) 1705 µL of distilled water were added. Zn^{2+} ion probe Fluozin-1 (500 µg, MW: 599.67 g mol^{-1}) was prepared in 833.8 µL distilled water. All stock solutions were kept desiccate and in dark conditions at –20 °C. The fluorescent probe stock solutions (1 mmol L^{-1}) were diluted to prepare different concentrations ranging from 1 to 50 µmol L^{-1}.

Fluorescence Measurements: The FLUOstar Galaxy microplate reader was used to assess the fluorescence intensity of the probes in aqueous solutions. Top excitation was executed, and the fluorescence emission data were analyzed in Excel. Metal ion solutions with the final concentration of 1–100 mmol L^{-1} prepared in Tris buffer (pH 4.0–9.0, 150 mmol L^{-1}) were mixed (1:1, v/v) with the four different fluorescent ion probes (1–50 µmol L^{-1}) and distributed in 96-well plates (black wall). The fluorescent probe (10 µL) was pipetted into the well plates followed immediately by 10 µL of ion solution. The probes were excited using top excitation (reflectance mode). A blank solution containing Tris buffer (pH 5.5–8.25, 150 mmol L^{-1}) and the fluorescent ion probes prepared in distilled water (1–50 µmol L^{-1}) mixed (1:1, v/v) were used for the calibration of the assays. The excitation and emission filters were chosen from the ones available from the microplate reader settings.

pH probes were distributed into 96 well plates and measured in the microplate reader with the following excitation and emission filters: $\lambda_{ex}/\lambda_{em}$: 520/590 nm. DMSO (a solvent that prevents hydrolysis) was mixed (1:1, v/v) with the probe solutions and used for the calibration of the assays, except for the ion selectivity test, where the sensor solution was mixed (1:1, v/v) with ion-free Tris buffer (pH 7.4 150 mmol L^{-1}) for calibration. For DA15C5, the measurements were conducted with the following excitation and emission filters: $\lambda_{ex}/\lambda_{em}$: 492/520 nm. For DA18C6, measurements were conducted with the following excitation and emission filters: $\lambda_{ex}/\lambda_{em}$: 340/505 nm. For Rhod-5N tripotassium salt ($\lambda_{ex}/\lambda_{em}$ = 551/576 nm) an emission filter of 540–512 nm and emission filter of 590 nm were used. The magnesium green pentapotassium salt probe ($\lambda_{ex}/\lambda_{em}$ = 506/531 nm) was exited with a 510–20 nm filter and emission was passed through a 550 nm filter. Mag-Fura-2 tetrapotassium salt Mg^{2+} ion probe ($\lambda_{ex}/\lambda_{em}$ = 330/505 nm) required UV-excitation. A 340 nm excitation light and a 500–510 nm emission filter were chosen for the readouts. The Zn^{2+} ion probe FluoZin-1 ($\lambda_{ex}/\lambda_{em}$ = 495/515 nm) used an A-492 nm filter excitation and the emission filter was chosen to 520 nm.

Scleral Lens Engraving: Due to its high accuracy and rapid fabrication process, a CO_2 laser was used to pattern hard scleral lenses (Ø = 16 mm) made mainly out of Paflufocon. Micro concavities with a 1.5 mm diameter were engraved using laser ablation at a power of 5.4 W and a beam speed of 3.1 mm s^{-1}. 1 µL of fluorescent ion probe followed by 1 µL of electrolyte solution were pipetted into the laser engraved cavity (Figures 1e, 2–6f, and 8a,b).

Enclosure of the Microfluidic Channels and Concavities in Scleral Lenses: Microconcavities were oxygen plasma treated (27–160 Pa, 100–300 W) for 60 s through a mask cut from a soft contact lens. Scleral lens sensors were sealed with a silicone hydrogel (30 µm, midafilcon) to enclose the microchannels.

Handheld Readout System and Image Analysis: To evaluate the analyte concentration in tear fluid with the algorithm a readout system was conceived. The portable black readout device was modeled in Catia VS for 3D printing. Three LEDs of 340, 505, and 555 nm were placed on rectangular prism blocks, which were located next to the interlayer of the device. The circuit equipment such as the resistors, cables, and switches were placed in the rectangular interlayer of the device. Three replaceable cover lid components were fabricated to fit the 530, 580, and 500 nm bandpass filters. A battery slot was carved into the bottom of the readout device to place the 6 V battery that powers the device. The 3D image was drawn in SketchUp.

The readout system consisted of a black 3D printed box in which the probe to be measured (the engraved scleral lens with the four ablated cavities and the sensors) was placed. The probe was excited with LEDs and the emission, passing through an adequate filter, was captured by a smartphone camera. The wavelength of the LED and the filter must be chosen differently for each fluorescent probe, since every sensor has specific excitation and emission wavelengths. The pictures captured by the smartphone camera were later used as an input for the readout algorithm, in which the image analysis took place.

Readout Algorithm and Application: A readout algorithm was implemented in MATLAB R2018b. As a first step, the algorithm was calibrated with images of the LED-excited sensors (Ca^{2+}, Mg^{2+}, or Zn^{2+}) at known concentrations. Once the calibration was done, the pH value had to be measured to make sure that the electrolytes to be analyzed were within the physiological range and thus showed a stable response. Given the pH value information, the MATLAB code calculated the fluorescence intensity of the analyte chosen by the user and gave the concentration as an output as well as a diagnostic result for dry eye disease, differentiating between dry eye subtypes and its severity stages. In the case of Mg^{2+} ion concentration assessment, additional information was needed. Since the Mg^{2+} ion sensor was not only sensitive to Mg^{2+} ions but also to Ca^{2+} and Zn^{2+} ions, hence their concentrations were needed to be known before calculating the Mg^{2+} ion concentration in the solution. Furthermore, a possible pH dependency of the sensor could also be deconvoluted by the algorithm. The prototype for an application called iCheck featuring the user interface with main functionalities was developed in Android Studio.

Supporting Information

Supporting Information is available from the Wiley Online Library or from the author.

Acknowledgements

The authors thank Martin Elsner, Alfred Michelfelder, and Oleskii Morgaienko for discussions and help in measurements. This research was funded by the Alexander von Humboldt Foundation and Carl Friedrich von Siemens Foundation.

Conflict of Interest

The authors declare no conflict of interest.

© 2019 The Authors. Published by WILEY-VCH Verlag GmbH & Co. KGaA, Weinheim

Keywords

biosensors, diagnostics, ophthalmology, scleral lenses, smartphones

Received: October 15, 2019
Revised: November 13, 2019
Published online: December 13, 2019

[1] G. N. Foulks, *Surv. Ophthalmol.* **2007**, *52*, 369.
[2] a) E. Goto, Y. Yagi, Y. Matsumoto, K. Tsubota, *Am. J. Ophthalmol.* **2002**, *133*, 181; b) K. K. Nichols, G. N. Foulks, A. J. Bron, B. J. Glasgow, M. Dogru, K. Tsubota, M. A. Lemp, D. A. Sullivan, *Invest. Opthalmol. Visual Sci* **2011**, *52*, 1922.
[3] M. Rolando, M. Zierhut, *Surv. Ophthalmol.* **2001**, *45*, S203.
[4] B. J. Mondino, S. I. Brown, *Arch. Ophthalmol.* **1976**, *94*, 1478.
[5] M. A. Lemp, G. N. Foulks, *Ocul. Surf.* **2007**, *5*, 75.
[6] R. Solans, J. A. Bosch, P. Galofre, F. Porta, J. Rosello, A. Selva-O'Callagan, M. Vilardell, *J. Nucl. Med.* **2001**, *42*, 738.
[7] W. D. Mathers, *CLAO J.* **2000**, *26*, 159.
[8] a) I. Toda, N. Asano-Kato, Y. Hori-Komai, K. Tsubota, *Arch. Ophthalmol.* **2002**, *120*, 1024; b) I. Toda, N. Asano-Kato, Y. Komai-Hori, K. Tsubota, *Am. J. Ophthalmol.* **2001**, *132*, 1.
[9] J. A. Hovanesian, S. S. Shah, R. K. Maloney, *J. Cataract Refractive Surg.* **2001**, *27*, 577.
[10] K. Tsubota, E. Goto, H. Fujita, M. Ono, H. Inoue, I. Saito, S. Shimmura, *Brit. J. Ophthalmol.* **1999**, *83*, 390.
[11] P. McCluskey, R. J. Powell, *Lancet* **2004**, *364*, 2125.
[12] M. Fujita, T. Igarashi, T. Kurai, M. Sakane, S. Yoshino, H. Takahashi, *Am. J. Ophthalmol.* **2005**, *140*, 808.
[13] A. J. Bron, *Surv. Ophthalmol.* **2001**, *45*, S221.
[14] R. Sivaraj, O. Durrani, A. Denniston, P. Murray, C. Gordon, *Rheumatology* **2007**, *46*, 1757.
[15] M. E. Stern, R. W. Beuerman, R. I. Fox, J. Gao, A. K. Mircheff, S. C. Pflugfelder, *Cornea* **1998**, *17*, 584.
[16] a) P. Versura, E. C. Campos, *Gynecol. Endocrinol.* **2005**, *20*, 289; b) A. Janine, *Ocul. Surf.* **2007**, *5*, 93.
[17] I. Kaiserman, N. Kaiserman, S. Nakar, S. Vinker, *Am. J. Ophthalmol.* **2005**, *139*, 498.
[18] a) O. D. Schein, B. Muno, J. M. Tielsch, K. Bandeen-Roche, S. West, *Am. J. Ophthalmol.* **1997**, *124*, 723; b) O. D. Schein, J. M. Tielsch, B. Muñoz, K. Bandeen-Roche, S. West, *Ophthalmology* **1997**, *104*, 1395.
[19] a) B. Chiang, P. Asbell, B. Franklin, *Invest. Ophthalmol. Visual Sci.* **1988**, *29*, 337; b) T. D. Rees, G. S. LaTrenta, *Plast. Reconstr. Surg.* **1988**, *82*, 619; c) O. Schirmer, *Graefe's Arch. Clin. Exp. Ophthalmol.* **1903**, *56*, 197.
[20] A. J. Bron, V. E. Evans, J. A. Smith, *Cornea* **2003**, *22*, 640.
[21] D. R. Korb, J. V. Greiner, J. Herman, *Cornea* **2001**, *20*, 811.
[22] a) J. P. Gilbard, R. L. Farris, *Acta Ophthalmol.* **1983**, *61*, 108; b) J. P. Gilbard, R. L. Farris, *Arch. Ophthalmol.* **1979**, *97*, 1642.
[23] V. Y. Bunya, N. M. Fuerst, M. Pistilli, B. E. McCabe, R. Salvo, I. Macchi, G. S. Ying, M. Massaro-Giordano, *JAMA Ophthalmol.* **2015**, *133*, 662.
[24] S. Chotikavanich, C. S. de Paiva, J. J. Chen, F. Bian, W. J. Farley, S. C. Pflugfelder, *Invest. Opthalmol. Visual Sci.* **2009**, *50*, 3203.
[25] a) L. Zhou, S. Z. Zhao, S. K. Koh, L. Chen, C. Vaz, V. Tanavde, X. R. Li, R. W. Beuerman, *J. Proteomics* **2012**, *75*, 3877; b) Y. Ohashi, R. Ishida, T. Kojima, E. Goto, Y. Matsumoto, K. Watanabe, N. Ishida, K. Nakata, T. Takeuchi, K. Tsubota, *Am. J. Ophthalmol.* **2003**, *136*, 291.
[26] a) M. Kawashima, K. Tsubota, *BMC Ophthalmol.* **2013**, *13*, 34; b) D. Finis, N. Pischel, S. Schrader, G. Geerling, *Cornea* **2013**, *32*, 1549.
[27] a) S. E. Moss, R. Klein, B. E. Klein, *Arch. Ophthalmol.* **2000**, *118*, 1264; b) C. G. Begley, B. Caffery, K. Nichols, G. L. Mitchell, R. Chalmers, *Lacrimal Gland, Tear Film, and Dry Eye Syndromes 3*, Springer, Boston, MA **2002**, p.1009.
[28] M. Moshirfar, K. Pierson, K. Hanamaikai, L. Santiago-Caban, V. Muthappan, S. F. Passi, *Clin. Ophthalmol.* **2014**, *8*, 1419.
[29] S. S. Lane, H. B. DuBiner, R. J. Epstein, P. H. Ernest, J. V. Greiner, D. R. Hardten, E. J. Holland, M. A. Lemp, J. E. McDonald, D. I. Silbert, *Cornea* **2012**, *31*, 396.
[30] A. M. Avunduk, M. C. Avunduk, E. D. Varnell, H. E. Kaufman, *Am. J. Ophthalmol.* **2003**, *136*, 593.
[31] a) D. R. Korb, J. V. Greiner, *Lacrimal Gland, Tear Film, and Dry Eye Syndromes*, Springer, New York **1994**, p. 293; b) L. T. Jones, *Am. J. Ophthalmol.* **1966**, *62*, 47.
[32] M. A. Lemp, *Am. J. Managed Care* **2008**, *14*, S88.
[33] a) G. Savini, P. Barboni, M. Zanini, *Am. J. Ophthalmol.* **2006**, *142*, 355; b) E. D. Donnenfeld, K. Solomon, H. D. Perry, S. J. Doshi, M. Ehrenhaus, R. Solomon, S. Biser, *Ophthalmology* **2003**, *110*, 1023.
[34] a) J. J. Nichols, L. T. Sinnott, *Invest. Opthalmol. Visual Sci* **2006**, *47*, 1319; b) C. G. Begley, B. Caffery, K. K. Nichols, R. Chalmers, *Optom. Vision Sci.* **2000**, *77*, 40.
[35] A. K. Yetisen, N. Jiang, A. Tamayol, G. U. Ruiz-Esparza, Y. S. Zhang, S. Medina-Pando, A. Gupta, J. S. Wolffsohn, H. Butt, A. Khademhosseini, S. H. Yun, *Lab Chip* **2017**, *17*, 1137.
[36] N. M. Farandos, A. K. Yetisen, M. J. Monteiro, C. R. Lowe, S. H. Yun, *Adv. Healthcare Mater.* **2015**, *4*, 792.
[37] R. Moreddu, D. Vigolo, A. K. Yetisen, *Adv. Healthcare Mater.* **2019**, *8*, 1900368.
[38] G. E. Dunbar, B. Y. Shen, A. A. Aref, *Clin. Ophthalmol.* **2017**, *11*, 875.
[39] a) H. Yao, A. J. Shum, M. Cowan, I. Lahdesmaki, B. A. Parviz, *Biosens. Bioelectron.* **2011**, *26*, 3290; b) J. Kim, M. Kim, M. S. Lee, K. Kim, S. Ji, Y. T. Kim, J. Park, K. Na, K. H. Bae, H. Kyun Kim, F. Bien, C. Young Lee, J. U. Park, *Nat. Commun.* **2017**, *8*, 14997.
[40] D. S. Jacobs, P. Rosenthal, *Cornea* **2007**, *26*, 1195.
[41] N. Jiang, Y. Montelongo, H. Butt, A. K. Yetisen, *Small* **2018**, *14*, 1704363.
[42] J. E. Whitaker, R. P. Haugland, F. G. Prendergast, *Anal. Biochem.* **1991**, *194*, 330.
[43] J. Reijenga, A. van Hoof, A. van Loon, B. Teunissen, *Anal. Chem. Insights* **2013**, *8*, 53.
[44] J. P. Gilbard, *Int. Ophthalmol. Clin.* **1994**, *34*, 27.
[45] G. W. Gokel, W. M. Leevy, M. E. Weber, *Chem. Rev.* **2004**, *104*, 2723.
[46] G. P. Amorino, M. H. Fox, *Cytometry* **1995**, *21*, 248.
[47] G. H. Zhang, J. E. Melvin, *J. Biol. Chem.* **1996**, *271*, 29067.
[48] A. Minta, R. Y. Tsien, *J. Biol. Chem.* **1989**, *264*, 19449.
[49] a) J. W. Putney, *Calcium Signaling*, CRC Press, Boca Raton, FL, USA **2005**; b) R. Y. Tsien, *Biochemistry* **1980**, *19*, 2396.
[50] N. J. Van Haeringen, *Surv. Ophthalmol.* **1981**, *26*, 84.
[51] R. E. London, *Annu. Rev. Physiol.* **1991**, *53*, 241.
[52] S. de la Fuente, R. I. Fonteriz, M. Montero, J. Alvarez, *Cell Calcium* **2012**, *51*, 65.
[53] E. R. H. Walter, M. A. Fox, D. Parker, J. A. G. Williams, *Dalton Trans.* **2018**, *47*, 1879.
[54] R. W. Sabnis, *Handbook of Biological Dyes and Stains: Synthesis and Industrial Applications*, John Wiley & Sons, New York, NY **2010**.
[55] R. Martinez-Zaguilan, J. Parnami, G. M. Martinez, *Cell. Physiol. Biochem.* **1998**, *8*, 158.
[56] H. Szmacinski, J. R. Lakowicz, *J. Fluoresc.* **1996**, *6*, 83.
[57] K. R. Gee, Z. L. Zhou, D. Ton-That, S. L. Sensi, J. H. Weiss, *Cell Calcium* **2002**, *31*, 245.
[58] A. R. Anderson, P. R. Kastl, Z. A. Karcioglu, *Brit. J. Ophthalmol.* **1987**, *71*, 212.
[59] Z. A. Karcioglu, *Surv. Ophthalmol.* **1982**, *27*, 114.
[60] Q. Han, Y. Fu, H. Zhou, Y. He, Y. Luo, *FEBS Lett.* **2007**, *581*, 3027.

© 2019 The Authors. Published by WILEY-VCH Verlag GmbH & Co. KGaA, Weinheim

[61] L. Zhu, Z. Yuan, J. T. Simmons, K. Sreenath, *RSC Adv.* **2014**, *4*, 20398.
[62] S. D. Meier, Y. Kovalchuk, C. R. Rose, *J. Neurosci. Methods* **2006**, *155*, 251.
[63] E. R. H. Walter, J. A. G. Williams, D. Parker, *Chem. - Eur. J.* **2018**, *24*, 7724.
[64] R. R. Hendrixson, M. P. Mack, R. A. Palmer, A. Ottolenghi, R. G. Ghirardelli, *Toxicol. Appl. Pharmacol.* **1978**, *44*, 263.
[65] P. Arenaz, L. Bitticks, K. H. Pannell, S. Garcia, *Mutat. Res. Genet. Toxicol.* **1992**, *280*, 109.
[66] J. P. Bergmanson, P. G. Soderberg, *Ophthalmic Physiol. Opt.* **1995**, *15*, 83.
[67] A. K. Yetisen, R. Moreddu, S. Seifi, N. Jiang, K. Vega, X. Dong, J. Dong, H. Butt, M. Jakobi, M. Elsner, A. W. Koch, *Angew. Chem., Int. Ed.* **2019**, *58*, 10506.
[68] W. H. Coles, P. A. Jaros, *Brit. J. Ophthalmol.* **1984**, *68*, 549.
[69] S. Y. Botelho, A. M. Goldstein, M. L. Rosenlund, *J. Pediatr.* **1973**, *83*, 601.
[70] K. Green, D. L. MacKeen, T. Slagle, L. Cheeks, *Ophthalmic Res.* **1992**, *24*, 99.
[71] R. Avisar, H. Savir, Y. Sidi, J. Pinkhas, *Invest. Ophthalmol. Visual Sci.* **1977**, *16*, 1150.

© 2019 The Authors. Published by WILEY-VCH Verlag GmbH & Co. KGaA, Weinheim